SECTION: Table_of_Contents_Chapter Chapter title in running head: CHAPTER 5. SPECIAL PROFILING TECHNIQUES... Chapter_ID: 8_II_5_en Part title in running head: PART II. OBSERVING SYSTEMS

SECTION: Chapter_book

Chapter title in running head: CHAPTER 5. SPECIAL PROFILING TECHNIQUES...

Chapter_ID: 8_II_5_en

Part title in running head: PART II. OBSERVING SYSTEMS

CHAPTER 5. SPECIAL PROFILING TECHNIQUES FOR THE BOUNDARY LAYER AND THE TROPOSPHERE

5.1 GENERAL

Special profiling techniques have been developed to obtain data at high temporal and spatial resolution which is needed for analysis, forecasting and research on the smaller meteorological scales and for various special applications. This chapter gives a general overview of current surface-based systems that can be used for these purposes. It is divided into two main parts: remote-sensing and in situ direct measuring techniques. Some of these techniques can be used for measurements over the whole troposphere, and others are used in the lower troposphere, in particular in the planetary boundary layer.

Remote-sensing techniques are based on the interaction of electromagnetic or acoustic energy with the atmosphere. The measuring instrument and the variable to be measured are spatially separated, as opposed to on-site (in situ) sensing. For atmospheric applications, the technique can be divided into passive and active techniques. Passive techniques make use of naturally occurring radiation in the atmosphere (microwave radiometers). Active systems (sodars, windprofilers, RASSs – radio acoustic sounding systems — and, lidars, and GNSS) are characterized by the injection of specific artificial radiation into the atmosphere. These surface-based profiling techniques are described in section 5.2. Other remote-sensing techniques relevant to this chapter are discussed in PartVolume III, Chapter 7, (Radar Measurements), and PartVolume IVII. (Space-Based Observations).

Section 5.3 describes in situ techniques with instruments located on various platforms to obtain measurements directly in the boundary layer (balloons, boundary layer radiosondes, instrumented towers and masts, instrumented tethered balloons). Chapters 12 and 13 in <u>PartVolume</u> I describe the more widely used techniques using balloons to obtain profile measurements.

The literature on profiling techniques is substantial. For general discussions and comparisons see Derr (1972), WMO (1980), Martner et al. (1993) and the special issue of the *Journal of Atmospheric and Oceanic Technology* (Volume 11, No. 1, 1994; see http://journals.ametsoc.org/toc/atot/11/1).

<u>Users should take note of the detailed information that comes with specific commercial</u> <u>measurement systems. In particular, most include advice about site selection, safety, and the</u> <u>comparative advantages of specific signal processing algorithms that can be turned on or off.</u>

5.2 SURFACE-BASED REMOTE-SENSING TECHNIQUES

5.2.1 Acoustic sounders (sodars)

Sodars (sound detection and ranging) operate on the principle of the scattering of acoustic waves by the atmosphere. According to the theory of the scattering of sound, a sound pulse emitted into the atmosphere is scattered by refractive index variations caused by small-scale turbulent temperature and velocity fluctuations, which occur naturally in the air and are particularly associated with strong temperature and humidity gradients present in inversions. In the case of backscattering (180°), only temperature fluctuations with a scale of one half of the transmitting acoustic wavelength determine the returned echo, while, in other directions, the returned echo is caused by both temperature and velocity fluctuations, except at an angle of 90°, where there is no scattering.

Useful references to acoustic sounding include Brown and Hall (1978), Neff and Coulter (1986), Gaynor et al. (1990) and Singal (1990).

A number of different types of acoustic sounders have been developed, but the two most common types considered for operational use are the monostatic sodar and the monostatic Doppler sodar.

A monostatic sodar consists of a vertically pointed pulsed sound source and a collocated receiver. A small portion of each sound pulse is scattered back to the receiver by the thermal fluctuations which occur naturally in the air. The receiver measures the intensity of the returned sound. As in a conventional radar, the time delay between transmitting and receiving an echo is indicative of the target's range. In a <u>bistaticbi-static</u> sodar, the receiver is located some distance away from the sound source to receive signals caused by velocity fluctuations.

As well as measuring the intensity of the return signal, a monostatic Doppler sodar also analyses the frequency spectrum of the transmitted and received signals to determine the Doppler frequency shift between transmitted and backscattered sound. This difference arises because of the motion of the temperature fluctuations with the air, and provides a measure of the radial wind speed of the air. A Doppler sodar typically uses three beams, one directed vertically and two tilted from the vertical to determine wind components in three directions. The vertical and horizontal winds are calculated from these components. The vector wind may be displayed on a time-height plot at height intervals of about 30 to 50 m.

The maximum height that can be reached by acoustic sounders is dependent on system parameters, but also varies with the atmospheric conditions. Economical systems can routinely reach heights of 600 m or more with height resolutions of a few tens of metres.

A sodar might have the following characteristics:

TABLE: Table as text NO space	
Parameter	Typical value
Pulse frequency	1 500 Hz
Pulse duration	0.05 to 0.2 s
Pulse repetition period	2 to 5 s
Beam width	15°
Acoustic power	100 W

Monostatic sodars normally produce a time-height plot of the strength of the backscattered echo signal. Such plots contain a wealth of detail on the internal structure of the boundary layer and can, in principle, be used to monitor inversion heights, the depth of the mixing layer – changes in boundary stability – and the depth of fog. The correct interpretation of the plots, however, requires considerable skill and background knowledge, and preferably additional information from in situ measurements and for the general weather situation.

Monostatic Doppler sodar systems provide measurements of wind profiles as well as intensity information. Such systems are a cost-effective method of obtaining boundary layer winds and are particularly suited to the continuous monitoring of inversions and winds near industrial plants where pollution is a potential problem.

The main limitation of sodar systems, other than the restricted height coverage, is their sensitivity to interfering noise. This can arise from traffic or as a result of precipitation or strong winds. This limitation precludes their use as an all-_weather system. Sodars produce sound, the nature and level of which is likely to cause annoyance in the near vicinity, and this may preclude their use in otherwise suitable environments.

CHAPTER 5. SPECIAL PROFILING TECHNIQUES FOR THE BOUNDARY LAYER AND THE TROPOSPHERE

Some systems rely upon absorbent foam to reduce the effect of external noise sources and to reduce any annoyance caused to humans. The physical condition of such foam deteriorates with time and must be periodically replaced in order to prevent deterioration in instrument performance.

5.2.2 Wind profiler radars

Wind profilers are very high and ultra high frequency. The term wind profiler is often used as an abbreviation for a whole class of Doppler radars which are specifically designed for measuring wind determining vertical profiles in all weather conditions. These radars of the wind. Unlike conventional weather radars, these instruments are able to make useful measurements even in the absence of precipitation and clouds. This clear air sensing capability is a truly unique feature of this radar. The use of wavelengths ranging from about 0.2 to 7 m (corresponding to frequencies between about 1300 and 40 MHz) makes it possible to detect signals backscatteredechoes scattered from radioirregularities of the refractive index irregularities associated with turbulent eddies with of air. If these have spatial scales of one half of the radar wavelength (the-, then constructive interference occurs and makes the return strong enough to be detectable (Bragg condition). As the turbulent eddies/Note that no clear air scattering is observed if the half-wavelength of the radar is smaller than the inner scale of turbulence, where refractive index irregularities vanish due to the dissipative effects of viscosity. In a first order approximation, the turbulent structures drift with the mean wind, their translational velocity provides of air, thus providing a direct measure of the mean-wind-vector.

Radar wind profilers not only receive electromagnetic waves backscattered at refractive index irregularities, but also echoes scattered from particles (mainly precipitation), airborne objects (birds, bats, airplanes) and clouds. Profilers typically measureeven from the plasma in lightning channels. Also, echoes from the ground can be received through antenna side lobes. The relative contribution of these differing scattering processes is a function of radar wavelength.

There are two techniques for wind measurements by radar wind profilers; namely the Doppler method and the spaced antenna method (Fukao et al., 2014), with most operational systems using the first method.

In the Doppler technique, the frequency shift, induced by the motion of the scattering matter along the line of sight of a particular beam direction, is measured and converted into a radial velocity-of the air in three or more directions —. The horizontal and vertical wind components are obtained from sequentially made radial wind measurements in at least three linearly independent directions. The wind vector retrieval is based on further assumptions on the wind field structure. Horizontal homogeneity and stationarity of the mean wind field allows for a simple closed-form expression of this algorithm (see Teschke and Lehmann (2017)). Simple Doppler-Beam-Swinging configurations use a vertically and pointing beam and about 2-4 oblique (about 15° off-vertical-in the north and east direction — and from these components they determine the horizontal and vertical wind components. Simpler systems may only measure the radial velocity in two-) beams. A higher number of off-vertical directions and, by assuming that the vertical air velocity is negligible, determine_beams yield generally to better results than the simple three-beam technique (Adachi et al., 2005). Other sampling configurations, like velocity-azimuth display (VAD), are also possible.

The spaced antenna technique uses a vertically pointing radar beam and at least three independent receiving vertically directed antennas. This allows for a correlation-based estimate of the wind speed based on the apparent motion of the backscattered interference or diffraction pattern on the ground. Corrections have to be made for temporal changes of the scattering structures to obtain an estimate of the horizontal wind velocity. The four beam profiler wind measurement technique is more practical than the three-beam profiler technique in that its measurement is not affected significantly by vertical wind (Adachi et al., 2005. Spaced antenna and Doppler techniques have comparative advantages and disadvantages, some of which are described in Dolman and Reid (2014).

For further discussion see Gossard and Strauch (1983), Hogg et al. (1983), Weber et al. (1990), Weber and Wuertz (1990) and WMO (1994).

The nature of the scattering mechanism requires wind profiler radars to function between 40 and 1 300 MHz. Performance deteriorates significantly at frequencies over 1 300 MHz. The The choice of operating frequency is influenced by depends on the required altitude coverage and resolution, but is strongly affected by regulatory constraints. In practice, most systems are built for the three

frequency bands (around 50 MHz, 400 MHz and 1 000 MHz) and these systems operate in low mode (shorter pulse: lower altitude) and high mode (longer pulse: higher altitude) which trade vertical range for resolutionidentified in the relevant regulatory decisions for spectrum allocation made by the World Radio Conference 1997 (Resolution 217, WRC-97). Obtaining the necessary frequency clearances (operating licenses) can be an administrative problem and radio-frequency interference (RFI) contaminations from other in-band radio services can lead to an additional challenge for the operation of a radar wind profiler. Typical characteristics are summarized in the table below.

TABLE: Table horizontal lines

Profiler parameter	Stratosphere	Troposphere	Lower troposphere	Boundary layer
Frequency (MHz)	50	400 <u>-500</u>	400 <u>-500</u>	1 000
Peak power (kW)	500	40	2	1
Operating height range (km)	3-30<u>2-20</u>	1<u>0.5</u>-16	0. 6-5<u>3-10</u>	0. <u>2-</u> 3 -2
Vertical resolution (m)	150 <u>-500</u>	150 <u>-500</u>	150 <u>-300</u>	50- 100<u>300</u>
Antenna type	Yagi array	Yagi-array or Cocc	Yagi array or Coco	Dish or phased array
Typical antenna size (m)	100×100	10×10	6×6	3×3
Effect of rain or snow	Small	Small in light rain	Small in light rain	Great

Profilers are able to operate unattended and to make continuous measurements of the wind almost directly above the site. These features are the principal advantages that profilers have over wind-measuring systems which rely on tracking balloons.

Any given profiler has both minimum and maximum ranges below and above which it cannot take measurements. The minimum range depends on the length of the transmitted pulse, the recovery time of the radar receiver and the strength of ground returns received from nearby objects. Thus, care must be taken in siting profilers so as to minimize ground returns. Sites in valleys or pits may be chosen so that only the ground at very short range is visible. These considerations are most important for stratospheric profilers. The extent of the ground clutter effects on higher frequency radars can be reduced by suitable shielding.

The

Radar wind profiler antennas typically employ a phase-array design with electronic beam steering, with the exception of a few mechanically steered dish-type antennas. The vertical resolution depends on the width of the transmitted pulse, and different pulse widths are typically used for specific low- and high-mode settings. Maximum height coverage is related to pulse width (through average power) so this choice trades range resolution for height coverage. Pulse compression methods are also frequently used to improve height coverage without compromising range resolution. These are generally effective, but can potentially generate self-clutter (Wakasugi and Fukao, 1985).

The minimum usable height range depends on the antenna size, the pulse width, the recovery time of the radar receiver and the strength of possible near-range ground clutter returns. Because ground clutter is quite variable, this minimum range can change with time and site.

<u>The strength of the received</u> signal received by profilers generally decreases with increasing height. This ultimately limits the height to which a given profiler can take measurements. <u>This can be taken</u>. <u>In contrast to the minimum range, the</u> maximum range is dependenta statistical quantity depending on <u>both</u> the characteristics of the radar andhardware and the state of the atmosphere. It typically increases with the product of the mean transmitter power and the antenna aperture, but is <u>mainly</u> subject to an absolutea physical (clear air scattering) limit determined by the radar frequency used. These factors mean that the large high powered stratospheric profilers are able to take measurements at the greatest heights. For a given profiler, however, the given by the used <u>CHAPTER 5. SPECIAL PROFILING TECHNIQUES FOR THE BOUNDARY LAYER AND THE TROPOSPHERE</u> <u>wavelength. The</u> maximum height varies considerably with the meteorological conditions; on <u>occasions there may be and gaps in the coverage at lower heights may sometimes occur</u>.

Because it is important to take measurements at the maximum height possible, profilers gather data for several minutes in order to integrate the weak signals obtained. Typically, a profiler may take 6 or 12 min to make the three sets of observations required to measure the wind velocity. In many systems, a set of such observations is combined to give an hourly measurement.

Because profilers are made to be sensitive to the very weak returns from atmospheric inhomogeneities, they can also detect signals from aircraft, birds and insects. In general, such signals confuse the profilers and may lead to erroneous winds being output. In these circumstances, a number of independent measurements will be compared or combined to give either an indication of the consistency of the measurements or reject spurious measurements.

In the 1 000 and 400 MHz bands, precipitation is likely to present a larger target than the refractive index inhomogeneities. Consequently, the measured vertical velocity is reflectivity-weighted and is not operationally useful.

Care must be taken in siting profilers so as to minimize ground returns and to avoid possible in-band radio frequency (RF) emissions of other radio services.

Large stratospheric profilers are expensive and require large antenna arrays, typically 100 m x 100 m, and relatively and high-power transmitters. Because they are large, it can be<u>It is therefore</u> difficult to find suitable sites for them, and their height resolution and minimum heights are not good enough for certain applications. They have the advantage of being able to take routinely make wind measurements to above about 20 km in height, and the measurements are unaffected by all but the heaviest of rainfall rates.

not strongly affected by precipitation. Tropospheric profilers operating in the 400–500 MHz frequency band are likely to be the most appropriate for synoptic and mesoscale measurements. They are of modest size and are relatively unaffected by rain.

the best compromise between height range covered and system size. Boundary layer profilers are less expensive and <u>can</u> use <u>rather</u> small antennas. Vertical velocity cannot be measured in rain, but raindropsTheir vertical height range for clear air measurements is typically limited to the lower atmosphere, however the useable vertical range can increase the radar cross section and actually increase the useful vertical range for the measurement of horizontal windsignificantly during precipitation, when scattering from hydrometeors becomes the dominant echoing mechanism.

The signal processing for Doppler wind profilers is similar to the processing employed in other Doppler radars. In contrast to weather radars, Doppler velocity resolution is typically better due to the longer dwell times, and the possibility of range and frequency aliasing can be fully avoided with a prudent sampling configuration. Since wind profilers are designed to receive the very weak returns from fluctuations of the refractive index, special algorithms for the filtering of ground and intermittent clutter echoes are mandatory. Intermittent clutter is comprised of unwanted echoes from aircraft, birds and insects. Especially migrating birds can lead to grossly erroneous wind estimates if intermittent clutter suppression is not implemented (Bianco et al., 2013).

Radial wind measurements can be made with a resolution of a few seconds. As hydrometeors present a more efficient radar target than refractive index inhomogeneities for most profiler wavelengths, the measured radial velocity can be a weighted average of air velocity and the velocities of scattering particles. Practical experience has demonstrated that the horizontal wind vector can be estimated with sufficient accuracy from both clear-air and particle scattering, since the scattering particles usually follow the horizontal wind field almost instantaneously. Thus, the horizontal wind can indeed be obtained in almost all weather conditions. Larger errors occur only if the implicit assumptions used in the wind estimation algorithm are violated. Note that the vertical wind can only be measured in a clear (particle-free) atmosphere.

Radar wind profilers are proven systems allowing for continuous, unattended operational measurements of the mean (upper-air) vertical wind profile directly above the site. The typical time resolution for a single wind profile ranges from about 10-60 minutes, depending on the instruments

characteristics and configuration. The positive impact of such data in NWP has been successfully demonstrated (see, e.g. Illingworth et al., 2015).

For further discussion see Gossard and Strauch (1983), Hogg et al. (1983), Weber et al. (1990), Weber and Wuertz (1990Profilers are active devices and obtaining the necessary frequency clearances is a serious problem in many countries. However, national and international allocation of profiler frequencies is actively being pursued.

), WMO (1994), Wilczak et al. (1996), Muschinski et al. (2005), Hocking (2011), Doviak and Zrnic (2014), Fukao et al. (2014) and Hocking et al. (2016).

5.2.3 Radio acoustic sounding systems

A radio acoustic sounding system is used to measure the virtual temperature profile in the lower troposphere. The technique consists in tracking a short high-intensity acoustic pulse that is transmitted vertically into the atmosphere by means of a collocated microwave Doppler radar. The measuring technique is based on the fact that acoustic waves are longitudinal waves that create density variations of the ambient air. These variations cause corresponding variations in the local index of refraction of the atmosphere which, in turn, causes a backscattering of the electromagnetic energy emitted by the microwave Doppler radar as it propagates through the acoustic pulse. The microwave radar measures the propagation speed of these refractive index perturbations as they ascend at the local speed of sound. The acoustic wavelength is matched to one half of the microwave wavelength (the Bragg condition), so that the energy backscattered from several acoustic waves adds coherently at the receiver, thus greatly increasing the return signal strength. By measuring the acoustic pulse propagation speed, the virtual temperature can be calculated as this is proportional to the square of the pulse propagation speed minus the vertical air speed.

The extensive literature on this technique includes May et al. (1990), Lataitis (1992*a*, 1992*b*) and Angevine et al. (1994).

A variety of experimental techniques have been developed to sweep the acoustic frequency and then to obtain a virtual temperature profile. A number of RASSs have been developed by adding an acoustic source and suitable processing to existing **profiler** windprofiler radars of the type mentioned above. For radar frequencies of 50, 400 and 1 000 MHz, acoustic frequencies of about 110, 900 and 2 000 Hz are required. At 2 000 Hz, acoustic attenuation generally limits the height coverage to 1 to 2 km. At 900 Hz, practical systems can reach 2 to 4 km. At 110 Hz, by using large 50 MHz profilers, maximum heights in the range of 4 to 8 km can be achieved under favourable conditions.

Comparisons with radiosondes show that, under good conditions, virtual temperatures can be measured to an accuracy of about 0.3 °C with height resolutions of 100 to 300 m. However, the measurements are likely to be compromised in strong winds and precipitation.

The RASS technique is a promising method of obtaining virtual temperature profiles. <u>It has been</u> <u>used operationally</u>, but <u>furtherhas known biases</u>. <u>Further</u> investigation is required before it can be used <u>operationally</u> with confidence over a height range, resolution and accuracy that respond to user requirements.

5.2.4 Microwave radiometers

Thermal radiation from the atmosphere at microwave frequencies originates primarily from molecular oxygen, water vapour, and liquid water and is dependent on their temperature and spatial distribution. For a gas such as oxygen, whose density as a function of height is well known, given the surface pressure, the radiation contains information primarily on the atmospheric temperature. Vertical temperature profiles of the lower atmosphere can be obtained by surface-based passive microwave radiometers measuring the microwave thermal emission by oxygen in a spectral band near 60 GHz. Spectral measurements in the 22–30 GHz upper wing of the pressure broadened water vapour absorption band provide information on the integrated amount of water vapour and liquid water, and the vertical distribution of water vapour. In addition, spectral measurements in both bands, combined with infrared cloud-base temperature measurements, provide information on the integrated amount and the vertical distribution of liquid water. For further information, see Hogg et al. (1983), Westwater et al. (1990), Solheim et al. (1998), Ware et al. (2003) and Westwater et al. (2005).

CHAPTER 5. SPECIAL PROFILING TECHNIQUES FOR THE BOUNDARY LAYER AND THE TROPOSPHERE

Individual downward-looking radiometersRadiometers operating at different frequencies are maximally sensitive to temperature at particular ranges of atmospheric pressure. The sensitivity as a function of pressure follows a bell-shaped curve (the weighting function). The frequencies of the radiometers are chosen so that the peaks in the weighting functions are optimally spread over the heights of interest. Temperature profiles above the boundary layer are calculated by means of numerical inversion techniques using measured radiations and weighting functions. The relatively broad width of the weighting function curves, and radiation from the terrestrial surfaceSpace-based radiometry, described in Volume IV, precludes accurate temperature profiles from being obtained near the surface and in the boundary layer when using space-based radiometer soundings. This is because of the relatively broad width of the weighting function curves, radiation from the terrestrial surface space based radiometer soundings. This is because of the relatively broad width of the weighting function curves, radiation from the terrestrial surface and in the boundary layer when using space-based radiometer soundings. This is because of the relatively broad width of the weighting function curves, radiation from the terrestrial surface and the fact that channels that are sensitive to the lower part of the atmosphere would also be sensitive to the skin temperature.

The principles of upward-looking radiometric temperature and humidity sounding from the terrestrial surface are well established. The temperature weighting functions of upward-looking profiling radiometers have narrow peaks near the surface that decrease with height. In addition, sensitivity to oxygen and water vapour emissions is not degraded by radiation from the terrestrial surface. This allows accurate temperature and humidity profile retrievals with relatively high resolution in the boundary layer and lower troposphere. On the other hand, the attenuation of microwave by the atmosphere, and the relatively broad width of the weighting function curves for channels sensitive to the upper part of the atmosphere, put a limit to the accuracy in retrieving temperature profiles above the boundary layer. Inversion techniques for upward-looking radiometers are based either on temperature and humidity climatology for the site that is typically derived from radiosonde soundings. The scanning configuration of microwave temperature profilers provides the highest resolution in the first few hundred metres. A multichannel system with fixed angle gives a better response at height greater than 1 km, but with a much coarser resolution (Cadeddu et al., 2002).radiosounding, or based on variational techniques on modelling the relation between the measured radiation, vertical temperature and humidity profiles.

Surface-based radiometers usually have a reduced accuracy in retrieving temperature profiles when it rains or snows. It is due to the accumulation of water, snow (Woods et al., 2005) or ice (Fernández-González et al., 2014) over the radome, lack of scattering and emission/absorption effects of precipitation in the retrieval algorithm, and enhanced microwave attenuation in the atmosphere by precipitation. The first issue can be remedied by using a hydrophobic radome and forcing airflow over the radiometer surface to avoid accumulation of water, snow and ice (Chan, 2009) or making the observations at an off-zenith angle to stay away from the thin films of water (Xu et al., 2014). For the second issue, it can be handled by incorporating observations from radar and parameterization of rain microphysics in the retrieval (Chan and Lee, 2015).

Surface-based and space-based radiometers are highly complementary. Space-based measurements provide coarse temporal and spatial resolution in the upper troposphere, and surface-based measurements provide high temporal and spatial resolution in the boundary layer and lower troposphere. Retrieved profiles from surface-based radiometers can be assimilated into numerical weather models to improve short term (1–12 h) forecasting by providing upper-air data in the interval between radiosonde soundings. Alternatively, raw brightness temperature from terrestrial radiometers can be assimilated directly into numerical weather models. This approach improves results by avoiding errors inherent in the profile retrieval process- and also allows for flow-dependent considerations in the assimilation. A similar method, which assimilates raw satellite radiometer radiances directly into weather models, demonstrated improved results years ago and is now widely used.

The main advantages of surface-based radiometers are their ability to produce continuous measurements in time, and their ability to measure cloud liquid. Continuous upper-air temperature, humidity and cloud liquid measurements can be used to improve nowcasting and short-term precipitation forecasting. <u>Changes in brightness temperature can also help to nowcast the on-set of convective events (Chakraborty et al., 2016).</u> These continuous measurements can be also used to detect the development or time of arrival of well-defined temperature changes (for studies of gas emissions, air pollution, urban heat islands, severe weather forecasting and warnings) (Kadygrov et al., 2003). Real-time radiometer data can also be used for alerting low level windshear events for aviation use (Chan and Lee, 2013).

Profiling radiometer reliability and accuracy have been widely demonstrated during long-term arctic, mid-latitude and tropical operations (Güldner and Spänkuch, 2001; Liljegren et al., 2005). The<u>One</u> result of the<u>based on</u> 13_-month operation of the Radiometrics MP3000months of operations (Gaffard and Hewison, 2003) shows that the root mean square value of the difference between the temperature observed by the radiosonde and that retrieved by the microwave radiometer ranges from 0.5 K (near the surface) to 1.8 K (at a height of 5 km). A second result (Güldner and Spänkuch (,_2001), who operated the Radiometrics TP/WVP-3000 for is based on 18 months of operations and compared radiometer retrievals with four radiosonde soundings daily, also. This shows a similar root mean square value from 0.6 K (near the surface) to 1.6 K (at a height of 7 km in summer and 4 km in winter). The root mean square value of water vapour profile is not more than 1 g m⁻³ in all altitudes (Gaffard and Hewison, 2003; Güldner and Spänkuch, 2001).

Terrestrial profiling radiometers demonstrate significant economic and practical advantage wheneverbenefits when lower tropospheric temperature, humidity and cloud liquid measurements with high temporal resolution are required, and where moderate vertical resolution is acceptable. Commercial profiling radiometer prices have dropped significantly over the past several years, and are now less than the typical annual cost of labour and materials for twice daily radiosonde soundings.

5.2.5 Laser radars (lidars)

Electromagnetic energy at optical and near-optical wavelengths (from ultraviolet through visible to infrared) generated by lasers is scattered by atmospheric gas molecules and suspended particles. Such scattering is sufficient to permit the application of the radar principle to make observations of the atmosphere by means of lidar (light detection and ranging). Optical scattering can generally be divided into inelastic and elastic. When the wavelength of the laser energy, scattered by atmospheric constituents, differs in wavelength from the incident laser wavelength, the process is called inelastic scattering. The most widely used inelastic scattering process used in experimental atmospheric lidar systems is Raman scattering, which results from an exchange of energy between incident photons and the molecular rotational and vibrational states of the scattering molecules. In elastic scattering processes, the incident and the scattered wavelengths are the same. This scattering may be Rayleigh or Mie scattering and depends on the species and size of particles with respect to the incident laser wavelength (see <u>PartVolume</u> III, Chapter 7). <u>Both for further description</u> of <u>theseRayleigh scattering</u>). <u>These</u> major scattering processes can occur simultaneously in the atmosphere.

For further reference see Hinkley (1976), WMO (1982), Thomas (1991) and Syed and Browell (1994).

The majority of lidars are operated in a monostatic mode, whereby the receiver is collocated with the laser transmitter. A typical lidar system uses a pulsed laser to transmit pulses of coherent light into the atmosphere. The average power of the laser used varies from a few milliwatts to tens of watts. An optical telescope mounted adjacent to the laser is used to capture the backscattered energy. The light collected by the telescope is focused onto a photomultiplier or photoconductive diode. The received information is normally made available on a display for real-time monitoring and is transferred to a computer for more detailed analysis.

The strength of the return signal is dependent both on the amount of scattering from the target and on the two-way attenuation between the lidar and the target — this attenuation depends on the proportion of the beam's energy scattered from its path and on the absorption by atmospheric gases. The scattering and absorption processes are exploited in different lidars to provide a variety of measurements.

Lidars based on elastic scattering (called Rayleigh or Mie lidars, or simply lidars), are mostly used for studies on clouds and particulate matter. The measurement of cloud-base height by a lidar is very straightforward; the rapid increase in the signal that marks the backscattered return from the cloud base can be readily distinguished; the height of the cloud base is determined by measuring the time taken for a laser pulse to travel from the transmitter to the cloud base and back to the receiver (see <u>PartVolume</u> I, Chapter 15).

Lidars are also used to detect the suspended particles present in relatively clear air and to map certain structural features such as thermal stability and the height of inversions. Natural

CHAPTER 5. SPECIAL PROFILING TECHNIQUES FOR THE BOUNDARY LAYER AND THE TROPOSPHERE

atmospheric particulate levels are sufficiently high in the lower atmosphere to allow lidars to measure air velocities continuously in the absence of precipitation, like weather radars. For the measurement of atmospheric wind, the most commonly used methods include pulsed and continuous-wave coherent Doppler wind lidar, direct-detection Doppler wind lidar and resonance Doppler wind lidar. The <u>annex to this chapterAnnex</u> discusses the requirements and performance test procedures for heterodyne pulsed Doppler lidar techniques.

Lidars can also be used to map and measure the concentration of man-made particulates, such as those originating from industrial stacks. Lidar observations have made very extensive and the <u>bestwell</u>-documented contributions to the study of stratospheric aerosol particulate concentration, which is strongly influenced by major volcanic eruptions and is an important factor in the global radiation balance.

It is much more difficult to obtain quantitative data on clouds, because of the variations in shape and distribution of droplets, water content, discrimination between water, ice and mixed phases, and the properties of suspended particles and aerosols. Indeed, such measurements require complex multiparameter research systems making several measurements simultaneously, using hypotheses concerning the optical properties of the medium, and complex mathematical data-reduction methods.

Differential absorption lidars (DIALs) work on the principle that the absorption coefficient of atmospheric gases varies greatly with wavelength. A DIAL system normally uses a laser that can be tuned between two closely-spaced frequencies, one which is strongly absorbed by a particular gas, and one which is not. The differences in the measurements as a function of range can be used to estimate the concentration of the gas under study. This is a most promising remote-sensing technique for the measurement of atmospheric composition and has been successfully used to measure concentrations of water, sulphur dioxide, nitrogen dioxide and, in particular, ozone.

The application of Raman scattering is of particular interest because the scattered radiation is frequency shifted by an amount which depends on the molecular species (Stokes lines). The strength of the backscattered signal is related to the species concentration. Raman lidars do not require a particular wavelength or tuned laser; laser wavelengths can be selected in a spectral region free from atmospheric absorption. By measuring the Raman spectrum, spatially resolved measurements can be taken of preselected atmospheric constituents, which have been used to obtain tropospheric profiles of water vapour, molecular nitrogen and oxygen, and minor atmospheric constituents. The main disadvantages are the lack of sensitivity over long ranges owing to the small scattering cross-sections and the requirement for high power lasers, which can lead to eye-safety problems in practical applications.

Lidar systems have provided a great deal of useful information for research studies but have had limited impact as operational tools. This is because they are relatively expensive and require very skilled staff in order to be developed, set up and operated. In addition, certain lidars are able to operate only under restricted conditions, such as in darkness or in the absence of precipitation.

5.2.6 Global Navigation Satellite System

The main purpose of the Global Navigation Satellite System (GNSS) is positioning, but since an atmospheric term influences the accuracy of the position estimate, meteorological content can be inferred from the estimated error. The time delay experienced by a signal originating from a satellite and measured by a receiver on Earth is related to the refractivity along the signal path, and thus also to the temperature and humidity along this path.

Meteorological information inferred from ground-based GNSS requires a surface network of GNSS receivers, a data connection and a processing facility. In general, a GNSS network of receivers is installed for land surveying purposes, and as a result close collaboration with national surveying institutes has been established in several countries. The collaboration is generally based on sharing sites and/or sharing information.

Additional information on processing techniques is available in WMO (2006*b*).

5.2.6.1 Description of the Global Navigation Satellite System

The GNSS consists of three segments: the space, the ground and the user segment. The space segment comprises a number of satellites in orbit. Currently four systems are deployed or are being deployed: GPS (United States), GLONASS (Russian Federation), Galileo (European Union) and Compass (China). GNSS satellites transmit time coded signals in a number of carrier wave frequencies which differ for different satellite systems.

The principle of GNSS is the same for all four systems. On-board atomic clocks control all signal components in the satellites. The ground segment controls the satellites for orbit adjustment and provides the broadcast ephemerides, which are disseminated to the user segment via the navigation message of the GNSS signal. A GNSS antenna and receiver (surface-based or space-borne) form the user segment. The receiver compares the time coded signal from the GNSS satellites with its own internal clock, from which the receiver can compute the pseudo ranges (*P*) to each satellite in view. When at least four pseudo ranges are observed the receiver can compute its position and its clock error. The standard positioning technique using the time coded signals has an accuracy of about 3–5 m.

The GNSS main observables are pseudo range (P) and carrier phase (L). For example, the GPS signals are broadcast at two different frequencies: namely L1 (1 575.42 MHz) and L2 (1 227.60 MHz). Both frequencies transmit P and L observables. Thus, for a dual-frequency receiver, four observables are available per epoch. Equations 5.1 and 5.2 present both P and L expressed as a sum of all error contributions forming the GNSS measurement, that is:

$$P = \rho + c \left(dt_{\text{rec}} - dt_{\text{sat}} \right) + \delta_{\text{rel}} + L_{\text{atm}} + I + K + M + \delta_{\text{tide}} + \varepsilon_P \quad (5.1)$$

$$L = \rho + c \left(dt_{\text{rec}} - dt_{\text{sat}} \right) + \delta_{\text{rel}} + L_{\text{atm}} - I + N \omega_L + K + M + \delta_{\text{tide}} + \varepsilon_L$$
5.2)

where *c* is the speed of light, ρ is the geometric distance between the satellite phase centre and the receiver phase centre, dt_{sat} is the satellite clock offset, dt_{rec} is the receiver clock offset, L_{atm} is the tropospheric delay, or slant total delay, due to the refractive nature of the atmosphere, *I* is the ionospheric delay along the ray path, δ_{rel} is the relativistic error, *K* is the receiver instrumental error, *M* is the multipath effect, δ_{tide} is the receiver position error due to polar tide, solid Earth tide and ocean loading, *N* is the ambiguity term (only relevant for carrier phase measurements, equation 5.2), ω_L is one wavelength contribution due to circular polarization of the signal and ε is the unmodelled noise error.

The observables have different uncertainty levels and different characteristics. In particular, phase measurements have a noise level of a few millimetres and are very accurate in comparison to pseudo range, which has an uncertainty of a few metres. Carrier phase is the primary and most important observable for low uncertainty parameter estimation, but pseudo-range observables are better suited for the observation and removal of specific receiver-related errors (multipath, etc.). Linear combination of the same kind of observable (*P* or *L*) measured at the two different frequencies is used to remove the first order of the ionosphere effect. Other techniques, such as double differencing, can remove the satellite and receiver clock error. However, this requires careful processing of the GNSS data.

5.2.6.2 Tropospheric Global Navigation Satellite System signal

The atmospheric excess path is caused by refraction and bending of the signal due to gradients in refractive index *n*. According to Fermat's principle, this excess path is:

$$L_{\text{atm}} = {}_{s} \int n \, ds - D + \Delta S \approx {}_{s} \int (n-1) ds \tag{5.3}$$

where $D (=_{s} \int ds)$ is the geometric distance and ΔS the excess path due to bending; the latter can be neglected for elevations larger than 10 degrees. The refractivity N is defined as N = 106 (n - 1) and, according to Smith and Weintraub (1953) and Thompson et al. (1986),

$$N = k_1 \rho R_d + (k_2 R_v - k_1 R_d + R_v / T k_3) \rho_w$$
(5.4)
= $N_h + N_w$

for the neutral atmosphere. Here, ρ is air density (kg m⁻³), ρ_w is water vapour density (kg m⁻³), *T* is temperature (K) and R_d = 287.05 J kg⁻¹ K⁻¹ and R_v = 461.51 J kg⁻¹ K⁻¹ are the gas constants for dry air and water vapour. The empirical constants are k_1 = 77.6 K hPa⁻¹, k_2 = 70.4 K hPa⁻¹ and k_3 = 373 900 K² hPa⁻¹ (Thayer, 1974). The first term in equation 5.4 is the hydrostatic refractivity, N_{hr} and the second term is called the wet refractivity, N_w .

Within a so-called network solution of GNSS data, the tropospheric delay is mapped to the zenith for all elevation and azimuth angles. In this way the number of unknowns is reduced and the position of the receiver can be estimated accurately. The mapped slant total delay to the zenith is called the zenith total delay (ZTD). When the precise position is estimated, an estimate of the atmospheric part of the signal can be retrieved. The ZTD can be considered as the sum of the zenith hydrostatic delay (ZHD) and the zenith wet delay (ZWD) (or, better, zenith non-hydrostatic delay). The integrals in the zenith direction of the hydrostatic and wet refractivity (expressed in metres) are:



5.2.6.3 Integrated water vapour

Zenith hydrostatic delay is related to the dry part of the atmosphere and, due to its stationary nature, can be estimated very accurately using the surface pressure measurements (p_s) and the location of the receiver (height *h* and latitude φ), using for example the Saastamoinen (1972) approximation, that is:

$$ZHD_{saas}(p_s, h, \varphi) = 2.2768 \cdot 10^{-5} p_s \left(1 - 2.66 \cdot 10^{-3} \cos(2\varphi) - 2.8 \cdot 10^{-7} h\right)^{-1}$$
(5.7)

The ZHD represents approximately 90_% of the entire tropospheric path delay. On the other hand, the ZWD cannot be sufficiently well modelled by surface data acquisition due to the irregular distribution of water vapour in the atmosphere. The ZWD can be rewritten as (following Davis et al., 1985):

$$ZWD = 10^{-6} \left[k_2 R_v - k_1 R_d + k_3 R_v \left(z \int \rho_w T^{-1} dz \right) \left(z \int \rho_w dz \right)^{-1} \right] z \int \rho_w dz$$
(5.8)

and by defining the weighted mean temperature as:

$$T_m = \left({}_z \int \rho_w \, dz \right) \left({}_z \int \rho_w \, T^{-1} \, dz \right)^{-1}$$
(5.9)

then:

$$ZWD = k'(T_m)_z \int \rho_w \, dz = k'(T_m) IWV$$
 (5.10)

where IWV is the vertically integrated column of water vapour overlying the GPS receiver. Based on, for example, radiosonde observations, the weighted mean temperature can be estimated by the surface temperature (T_s) , that is $k'(T_m) \approx k(T_s)$ (Bevis et al., 1994). Thus, the IWV can be estimated using the estimated ZTD, surface pressure (p_s) , antenna height (h) and latitude (φ) of the receiver:

$$IWV = k (T_s)^{-1} (ZTD - ZHD_{saas} (p_s, h, \varphi))$$
 (5.11)

The value of $k(T_s)$ is approximately 6.5 kg m⁻³.

5.2.6.4 Measurement uncertainties

Since ZTD is estimated, its accuracy depends on the method used, the accuracy of a priori information used, the stability of the receiver position and many other things. For example, the accuracy of the position of the satellite orbits will in general be higher after approximately 14 days when the so-called final orbits are available. Therefore, a distinction has to be made between near-real-time and post-processed estimates of ZTD. The accuracy of IWV is obviously closely related to the accuracy of the ZTD estimate.

The measurement uncertainty of near-real-time estimates is about 10 mm. For post-processed estimates, this value is about 5 to 7 mm. The measurement uncertainty of IWV is dependent on the total amount of water vapour and is of the order of $5_{-}-10_{-}$ (Elgered et al., 2004). The mean values have a clear seasonal signature: at mid latitudes very low values can be observed in winter (below 5 kg m⁻²) and values of 40 kg m⁻² can be seen during summer. In the tropics, values higher than 50 kg m⁻² are not uncommon.

5.3 IN SITU MEASUREMENTS

5.3.1 Balloon tracking

Balloon tracking is frequently used to obtain boundary layer winds and is usually performed by optical theodolites or a tracking radar. PartVolume I, Chapter 13, gives a more general account of windfinding.

When making lower tropospheric soundings, it is desirable to use a slow rate of balloon ascent in order to give high vertical resolution. The reduced rate of ascent may be achieved either by means of a brake parachute or by a reduced free lift.

For radar tracking, a small radar reflector is suspended below the balloon. For lower tropospheric soundings, the radar should be able to provide data at ranges as short as 100 m, and ideally the launch point must be farther away from the radar in a downwind direction than this minimum range.

A basic wind measurement can be taken using a single optical theodolite, but, in order to obtain reasonably accurate winds, a two-theodolite system is required. The baseline between the theodolites should exceed 1 km. In order to facilitate the sounding procedure and to ensure height accuracy, the theodolites should be equipped with computer interfaces so that the data can be logged and the necessary calculations performed in a timely manner. Under good conditions, wind profiles can be obtained up to an altitude of 3 000 m. However, the technique fails in adverse conditions such as precipitation, low cloud or fog.

It is, of course, possible to obtain additional wind data in the lower atmosphere using conventional radiosondes by taking more frequent tracking measurements in the first few minutes of a normal full sounding, for example, between 2 and 10 per minute.

5.3.2 Boundary layer radiosondes

Conventional radiosonde systems are described in detail in PartVolume I, Chapter 12. Special radiosondes have been designed specifically to make detailed observations of the boundary layer and lower troposphere. They differ from conventional radiosondes in that the sensors have greater sensitivity and faster response rates. Such radiosondes are used to measure temperature, humidity and wind profiles in the layer from the surface to elevations of typically 3 to 5 km.

The vertical ascent rate of these radiosondes is usually arranged to be between 150 and 200 m min⁻¹, which is rather slower than conventional radiosondes. The slower rate of ascent allows more detailed vertical profiles to be produced. The rate of ascent is normally determined by selecting an appropriately sized balloon, but may be modified by the use of a trailing brake parachute.

CHAPTER 5. SPECIAL PROFILING TECHNIQUES FOR THE BOUNDARY LAYER AND THE TROPOSPHERE

Because these instruments are required only to reach a limited height, they can normally be carried by a pilot balloon. In other respects, the sounding procedures and data processing are similar to those employed by standard radiosondes.

For soundings to an altitude of no more than 2 000 m, the pressure sensor is sometimes dispensed with, which results in a simpler and less expensive radiosonde. Even simpler systems are available which measure temperature only.

The basic requirements for boundary layer radiosondes are as follows¹:

TABLE: Table horizontal lines

Variable	Operating range	Resolution
Pressure	1 050 to 500 hPa	±0.5 hPa
Temperature	+40 <mark>℃-</mark> to -40 °C	±0.1 K
Humidity	100 % to 20 (or 10)%<u>)</u> %	±2_%
Wind speed	0.5 to 60 m s ^{-1}	±0.5 m s ⁻¹
Wind direction	0° to 360°	±5°

Measurements are typically taken at least every 30 s to give a vertical resolution of 50 to 100 m.

5.3.3 Instrumented towers and masts

Special instrumented towers and masts are used for many purposes, especially for the estimation of the diffusion of atmospheric pollution. A discussion is provided by Panofsky (1973).

For some purposes, the height of the tower must be up to 100 m, and for air-pollution monitoring and control projects it should exceed the height of the important sources of pollution by at least 50 m.

Measurements of temperature, humidity and wind should be made at several (at least two or three) levels, the lowest of which should be at the level of standard meteorological screen, close to the tower or mast. The number of measuring levels depends upon both the task and the height of the tower or mast. The use of just two levels provides no information on the shape of the vertical profile of meteorological variables and is, thus, very limiting. The number of measuring levels is usually greater for research projects than for routine use.

Usually, the data are processed and presented automatically together with differences between the levels that are provided to characterize the meteorological conditions. If the data are to be used directly by non-meteorological staff – such as those concerned with keeping concentrations of air pollutants within safe limits – they are often processed further by computer to provide derived data which are easily applied to the task in hand.

The sensors most commonly used for measurements on towers or masts are as follows:

- (a) Temperature: electrical resistance or thermocouple thermometers in screens, with or without aspiration;
- (b) Humidity: psychrometers, electrochemical or electromechanical sensors in screens;

¹ These requirements for boundary layer profile measurements differ from requirements for surface measurements in Volume I, Chapter 1, Annex A.

(c) Wind: cup and vane, propeller, sonic or hot-wire devices.

All sensors should have linear or linearized characteristics and their time constants should be small enough to ensure that the data gathered will adequately reflect local changes in the meteorological variables.

It is important that the structure of the tower or mast should not affect the sensors and their measurements appreciably. For open structures, booms – whether stationary or retractable – should be at least 2 m long, and preferably long enough to keep the sensors at least 10 tower diameters removed from the tower or mast. For solid structures, or where the required booms would not be practicable, a double system is required at each level, with booms on opposite sides of the tower or mast extending for at least three times the structure diameter. Measurements at a given time are then taken from the sensors exposed to the undisturbed wind.

Sometimes, in special situations, towers can be used to gather meteorological profile data without the direct mounting of fixed sensors; rather, a simplified method of sounding is used. A pulley is fastened at the highest possible point and a closed loop of rope extending to ground level is used to carry a radiosonde up and down the levels required by means of a hand- or motor-operated winch. The radiosonde, which is modified to include wind sensors, transmits its data to an appropriate receiving system at ground level. Much more vertical detail is possible than that provided by a boom installation, and the altitudes of significant features can be determined. However, sustained observation is possible at only a single level.

For an accurate definition of the extent of pollution dispersion in certain weather conditions, the tower height may be too limited. In such circumstances, unless a radiosonde station is within about 50 km, a special radiosonde is provided at the site of the tower or mast for making local soundings up to an altitude of about 3 000 m. In addition to their main purpose, the data obtained can be treated as complementary to those of the basic aerological network, and can also be used in more detailed investigations of local weather phenomena.

Tower measuring equipment requires periodical checking by highly qualified instrument maintenance staff who should pay special attention to the state and performance of sensors and recorders and the connecting cables, sockets and plugs exposed to outdoor weather conditions.

5.3.4 Instrumented tethered balloons

Typical applications of instrumented tethered balloons include the measurement of temperature, humidity and wind profiles (and their short-period changes) from the surface to an altitude of about 1 500 m, and longer-period investigation of the meteorological conditions at one or more selected levels. The sensors are suspended in one or more packages beneath the balloon, or clamped to the tethering cable. The sensor's response is normally telemetered to the ground either by radio, or by conductors incorporated into the tethering cable. The techniques are discussed by Thompson (1980).

Tethered-balloon systems tend to use either large (~600 m³) or small (~10 to 100 m³) balloons. The small balloons are normally used to obtain profiles, and the larger ones to obtain measurements at multiple levels. Tethered balloons should be designed for low drag and to ride steadily. They are usually inflated with helium. Larger balloons should be able to carry a load of up to 50 kg (in addition to the tethering cable) to an altitude of 1 500 m. The balloon should be capable of operation at wind speeds of up to 5 m s⁻¹ at the surface and 15 m s⁻¹ at altitudes within the operational range. The tethering cable of a large balloon should be able to withstand a force of 2 000 to 3 000 kg to avoid a breakaway (200 to 300 kg for smaller balloons).

Tethered-balloon flying is subject to national rules concerning aviation safety. For this reason and for the convenience of the operating staff, the use of balloons which have distinct colours and night-warning lights is highly recommended. An automatic device for the rapid deflation of the balloon is mandatory, while a metallized radar target suspended below the balloon is optional.

The main factors limiting tethered-balloon operation are strong wind speed aloft, turbulence near the surface and lightning risk.

The winch used to control the balloon may be operated electrically or by hand. At least two speeds (e.g. 1 and 2 m s^{-1}) should be provided for the cable run. In addition, the winch should be equipped

CHAPTER 5. SPECIAL PROFILING TECHNIQUES FOR THE BOUNDARY LAYER AND THE TROPOSPHERE

with a hand-brake, a cable-length counter and a tension gauge. The winch should be electrically earthed, whether electrically operated or not, as protection against atmospheric discharges.

The use of conductors to convey the sensor signals back to the ground is undesirable for a number of reasons. In general, it is preferable to use special radiosondes. Such radiosondes will have better resolution than those normally employed for free flights. The temperature and humidity sensors must have a horizontal shield to provide protection against solar radiation and rainfall, while allowing for adequate ventilation. Extra sensors are needed for wind speed and direction.

The basic requirements are the following²:

TABLE: Table horizontal lines

Variable	Operating range	Resolution	
Pressure	1 050 to 850 hPa	±0.5 hPa	•
Temperature	+40	±0.1 K	
Humidity	100 % to 20 (or 10)%<u>)</u> %	±2_%	3
Wind speed	0.5 to 15 m s^{-1}	±0.5 m s⁻¹	
Wind direction	0° to 360°	±1°	

For telemetry, one of the standard radiosonde frequencies may be used; the 400 MHz allocation is a frequent choice. The maximum weight, including the battery, should be within the load capability of the balloon; a limit of 5 kg is reasonable. The radiosonde should be suspended at least three balloon diameters below the balloon in a stable condition so that adequate shielding and ventilation are maintained.

A major problem encountered in the measurement of turbulent, rather than mean, quantities is the effect of cable vibration and balloon motion on the measurements. Special techniques have to be used for such measurements.

The ground-based equipment must include a receiver and recorder. The data are usually processed with the aid of a small computer.

Soundings can be performed during the ascent and descent of the balloon, either continuously or with pauses at selected levels. For the lower levels, height can be estimated from the length of the cable paid out, but at higher levels this method is no more than an approximation and an alternative is necessary. This takes the form of a calculation by means of the hydrostatic equation, using the observed distribution of pressure, temperature and humidity. Thus, the increment in geopotential metres from level n to level n+1 is given by:

$$29.27 T_v \ln(p_n / p_{n+1}) \tag{5.12}$$

where T_v is the mean of the virtual temperatures at levels *n* and *n*+1; and *p_n* and *p_{n+1}* are the two associated pressures. If conversion from geopotential to geometric height is required, this is readily done by using the Smithsonian meteorological tables; however, this is unlikely to be necessary. The height of the station barometer is taken as the datum for these calculations.

If the meteorological variables are observed using the level-by-level method, a few measuring cycles should be taken at each level, with the time required for stabilization being 2 to 3 min. In this way, the whole sounding sequence could take from a half to one whole hour. As for all radiosondes, a

² These requirements for boundary layer profile measurements differ from requirements for surface measurements in Volume I, Chapter 1, Annex A.

baseline check in a control screen should be made just before use, to establish the differences with a barometer and an aspirated psychrometer. A similar check should also be made just after the sounding is completed. Again, as for regular radiosonde ascents, the station-level data should be obtained not from the radiosonde data, but from conventional instruments in a standard station screen.

For the sounding data, pressure, temperature and humidity should be averaged at each level. For wind speed, the average should be calculated for a period of 100 or 120 s. If wind direction is not measured directly, it can be roughly estimated from the orientation of the balloon's longitudinal axis with respect to the north. The uncertainty of this method is $\pm 30^{\circ}$.

It should be stressed that operators must advise air traffic authorities of their plans and obtain permission for each sounding or series of soundings using tethered balloons.

SECTION: Chapter_book Chapter title in running head: CHAPTER 5. SPECIAL PROFILING TECHNIQUES... Chapter_ID: 8_II_5_annex_en

Part title in running head: PART II. OBSERVING SYSTEMS

ANNEX₇ GROUND-BASED REMOTE-SENSING OF WIND BY HETERODYNE PULSED DOPPLER LIDAR

(The text of the common ISO/WMO standard 28902-2:2017(E))

INTRODUCTION

Lidars (light detection and ranging), standing for atmospheric lidars in the scope of this annex, have proven to be valuable systems for remote-sensing of atmospheric pollutants, of various meteorological parameters such as clouds, aerosols, gases and (where Doppler technology is available) wind. The measurements can be carried out without direct contact and in any direction as electromagnetic radiation is used for sensing the targets. Lidar systems, therefore, supplement the conventional in situ measurement technology. They are suited for a large number of applications that cannot be adequately performed by using in situ or point measurement methods.

There are several methods by which lidar can be used to measure atmospheric wind. The four most commonly used methods are pulsed and continuous-wave coherent Doppler wind lidar, direct-detection Doppler wind lidar and resonance Doppler wind lidar (commonly used for mesospheric sodium layer measurements). For further reading, refer to references [1] and [2].

This annex³ describes the use of heterodyne pulsed Doppler lidar systems. Some general information on continuous-wave Doppler lidar can be found in Attachment A. An International Standard on this method is in preparation.

1. SCOPE

This annex specifies the requirements and performance test procedures for heterodyne pulsed Doppler lidar techniques and presents their advantages and limitations. The term "Doppler lidar" used in this annex applies solely to heterodyne pulsed lidar systems retrieving wind measurements from the scattering of laser light onto aerosols in the atmosphere. Their performances and limits are described based on standard atmospheric conditions.

³ Whereas this is referred to as an annex in the *Guide to Meteorological Instruments and Methods of Observation* (WMO-No. 8), it is referred to as a standard in the ISO document.

This annex describes the determination of the line-of-sight wind velocity (radial wind velocity).

Note: Derivation of wind vector from individual line-of-sight measurements is not described in this annex since it is highly specific to a particular wind lidar configuration. One example of the retrieval of the wind vector can be found in Attachment B.

This annex does not address the retrieval of the wind vector.

This annex may be used for the following application areas:

- (a) Meteorological briefing for, e.g. aviation, airport safety, marine applications and oil platforms;
- (b) Wind power production, e.g. site assessment and power curve determination;
- (c) Routine measurements of wind profiles at meteorological stations;
- (d) Air pollution dispersion monitoring;
- (e) Industrial risk management (direct data monitoring or by assimilation into micro-scale flow models);
- (f) Exchange processes (greenhouse gas emissions).

This annex addresses manufacturers of heterodyne pulsed Doppler wind lidars, as well as bodies testing and certifying their conformity. Also, this annex provides recommendations for the users to make adequate use of these instruments.

2. NORMATIVE REFERENCES

There are no normative references in this annex.

3. TERMS AND DEFINITIONS

For the purposes of this annex, the following terms and definitions apply.

- *Data availability*: Ratio between the actual considered measurement data with a predefined data quality and the number of expected measurement data for a given *measurement period*;
- *Displayed range resolution*: Constant spatial interval between the centres of two successive *range gates*;

Note: The displayed range resolution is also the size of a range gate on the display. It is determined by the range gate length and the overlap between successive gates.

Effective range resolution: Application-related variable describing an integrated range interval for which the target variable is delivered with a defined uncertainty;

Source: ISO 28902-1:2012, term 3.14

Effective temporal resolution: Application-related variable describing an integrated time interval for which the target variable is delivered with a defined uncertainty;

Source: ISO 28902-1:2012, term 3.12, modified

Extinction coefficient, *α*: Measure of the atmospheric opacity, expressed by the natural logarithm of the ratio of incident light intensity to transmitted light intensity, per unit light path length;

Source: ISO 28902-1:2012, term 3.10

Integration time: Time spent in order to derive the line-of-sight velocity;

Maximum acquisition range, R_{MaxA} : Maximum distance to which the lidar signal is recorded and processed;

Note: It depends on the number of acquisition points and the sampling frequency.

Maximum operational range, R_{MaxO} : Maximum distance to which a confident wind speed can be derived from the lidar signal;

Notes:

- 1. The maximum operational range is less than or equal to the maximum acquisition range.
- 2. The maximum operational range is defined along an axis corresponding to the application. It is measured vertically for vertical wind profiler. It is measured horizontally for scanning lidars able to measure in the full hemisphere.
- 3. The maximum operational range can be increased by increasing the measurement period and/or by downgrading the range resolution.
- 4. The maximum operational range depends on lidar parameters but also on atmospheric conditions.

Measurement period: Interval of time between the first and last measurements;

Minimum acquisition range, *R*_{MinA}: Minimum distance from which the lidar signal is recorded and processed;

Note: If the minimum acquisition range is not given, it is assumed to be zero. It can be different from zero, when the reception is blind during the pulse emission.

Minimum operational range, R_{MinO} : Minimum distance where a confident wind speed can be derived from the lidar signal;

Notes:

- 1. The minimum operational range is also called blind range.
- 2. In pulsed lidars, the minimum operational range is limited by the stray light in the lidar during pulse emission, by the depth of focus, or by the detector transmitter/receiver switch time. It can depend on pulse duration (T_p) and range gate width.

Physical range resolution: Width (FWHM) of the range weighting function;

Range gate: Width (FWHM) of the weighting function selecting the points in the time series for spectral processing and wind speed computation;

Notes:

- 1. The range gate is centred on the measurement distance.
- 2. The range gate is defined in number of bins or equivalent distance range gate.
- *Range resolution*: Equipment-related variable describing the shortest range interval from which independent signal information can be obtained;

Source: ISO 28902-1:2012, term 3.13

Range weighting function: Weighting function of the radial wind speed along the line of sight;

Temporal resolution: Equipment-related variable describing the shortest time interval from which independent signal information can be obtained;

Source: ISO 28902-1:2012, term 3.11

Velocity bias: Maximum instrumental offset on the velocity measurement;

Note: The velocity bias has to be minimized with adequate calibration, for example, on a fixed target.

Velocity range: Range determined by the minimum measurable wind speed, the maximum measurable wind speed and the ability to measure the velocity sign, without ambiguity;

Note: Depending on the lidar application, velocity range can be defined on the radial wind velocity (scanning lidars) or on horizontal wind velocities (wind profilers).

Velocity resolution: Instrumental velocity standard deviation;

Note: The velocity resolution depends on the pulse duration, the carrier-to-noise ratio and integration time.

Wind shear: Variation of wind speed across a plane perpendicular to the wind direction.

4. FUNDAMENTALS OF HETERODYNE PULSED DOPPLER LIDAR

4.1 Overview

A pulsed Doppler lidar emits a laser pulse in a narrow laser beam (see Figure 5.A.1). As it propagates in the atmosphere, the laser radiation is scattered in all directions by aerosols and molecules. Part of the scattered radiation propagates back to the lidar; it is captured by a telescope, detected and analysed. Since the aerosols and molecules move with the atmosphere, a Doppler shift results in the frequency of the scattered laser light.

At the wavelengths (and thus frequencies) relevant to heterodyne (coherent) Doppler lidar, it is the aerosol signal that provides the principal target for measurement of the backscattered signal.

The analysis aims at measuring the difference, Δf , between the frequencies of the emitted laser pulse, f_t , and of the backscattered light, f_r . According to the Doppler's equation, this difference is proportional to the line-of-sight wind component, as shown in formula 5.A.1:

$$\Delta f = f_{\rm r} - f_{\rm t} = -2v_{\rm r} / \lambda \tag{5.A.1}$$

where:

λ is the laser wavelength;

 v_r is the line-of-sight wind component (component of the wind vector, $\frac{r}{v}$, along the axis of laser beam, counted positive when the wind is blowing away from the lidar).

ELEMENT 1: Floating object (Automatic) ELEMENT 2: Picture inline fix size Element Image: 8_II_5-A1_en.eps END ELEMENT



END ELEMENT

The measurement is range resolved as the backscattered radiation, received at time t after the emission of the laser pulse, has travelled from the lidar to the aerosols at range x and back to the lidar at the speed of light, c. Formula 5.A.2 shows the linear relationship between range and time.

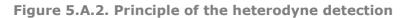
$$x = c \cdot \frac{t}{2} \tag{5.A.2}$$

4.2 Heterodyne detection

In a heterodyne lidar, the detection of the light captured by the receiving telescope (at frequency $f_r = f_t + \Delta f$) is described schematically in Figure 5.A.2. The received light is mixed with the beam of a highly stable, continuous-wave laser called the local oscillator. The sum of the two electromagnetic waves – backscattered and local oscillator – is converted into an electrical signal by a quadratic detector (producing an electrical current proportional to the power of the electromagnetic wave

illuminating its sensitive surface). An analogue high-pass filter is then applied for eliminating the low-frequency components of the signal.

ELEMENT 3: Floating object (Automatic) ELEMENT 4: Picture inline Element Image: 8_II_5-A2_en.eps END ELEMENT



END ELEMENT

The result is a current, i(t), beating at the radio frequency, $f_t + \Delta f - f_{lo}$:

$$i(t) = 2 \cdot \frac{\eta \cdot e}{h \cdot f_t} \cdot K \cdot \xi(t) \cdot \sqrt{\gamma(t) \cdot P_r(t) \cdot P_{lo}} \cdot \cos(2\pi(\Delta f + f_t - f_{lo}) \cdot t + \varphi(t)) + n(t)$$
(5.A.3)

 $i_{het}(t)$

where:

- *t* is the time;
- *h* is the Planck constant;
- η is the detector quantum efficiency;
- *e* is the electrical charge of an electron;
- *K* is the instrumental constant taking into account transmission losses through the receiver;
- $\xi(t)$ is the random modulation of the signal amplitude by speckles effect (see section 4.5.4);
- $\gamma(t)$ is the heterodyne efficiency;
- $P_{\rm r}(t)$ is the power of the backscattered light;
- $P_{\rm lo}$ is the power of the local oscillator;
- $f_{\rm lo}$ is the frequency of the local oscillator;
- $\varphi(t)$ is the random phase;
- n(t) is the white detection noise;

 $i_{\rm het}(t)$ is the heterodyne signal.

The heterodyne efficiency, $\gamma(t)$, is a measure for the quality of the optical mixing of the backscattered and the local oscillator wave fields on the surface of the detector. It cannot exceed 1. A good heterodyne efficiency requires a careful sizing and alignment of the local oscillator relative to the backscattered wave. Optimal mixing conditions are discussed in reference [3]. The heterodyne efficiency is not a purely instrumental function; it also depends on the refractive index turbulence (Cn²) along the laser beam (see reference [4]). Under conditions of strong atmospheric turbulence, the effect on varying the refractive index degrades the heterodyne efficiency. This can happen when the lidar is operated close to the ground during a hot sunny day.

In formula 5.A.4, $P_r(t)$ is the instantaneous power of the backscattered light. It is given by the lidar equation (see reference [3]):

$$P_{r}(t) = A \cdot \int_{0}^{+\infty} x^{-2} \cdot G(x) \cdot g\left(t - \frac{2x}{c}\right) \cdot \beta(x) \cdot \tau^{2}(x) dx \qquad (5.A.4)$$

with

$$\tau(x) = \exp\left[-\int_{0}^{x} \alpha(\zeta) d\zeta\right]$$

where:

- *x* is the distance to the lidar;
- *A* is the collecting surface of the receiving telescope;
- G(x) is the range-dependent sensitivity function ($0 \le G(x) \le 1$) taking into account, for example, the attenuation of the receiver efficiency at short range to avoid the saturation of the detector;
- g(t) is the envelope of the laser pulse power ($\int g(t) dt = E_0$, with E_0 as the energy of the laser pulse);

 $\beta(x)$ is the backscatter coefficient of the probed atmospheric target;

 $\tau(x)$ is the atmospheric transmission as a function of the extinction coefficient, α .

4.3 Spectral analysis

The retrieval of the radial velocity measurement from heterodyne signals requires a frequency analysis. This is done in the digital domain after analogue-to-digital conversion of the heterodyne signals. An overview of the processing is given in Figure 5.A.3. The frequency analysis is applied to a time window $(t, t + \Delta t)$ and is repeated for a number, N, of lidar pulses. The window defines a range gate $(x, x + \Delta x)$ with $x = c \cdot t / 2$ and $\Delta x = c \cdot \Delta t / 2$. N is linked to the integration time, $t_{int} = 1/f_{PRF}$, of the measurement (f_{PRF} is the pulse repetition frequency). The signal analysis consists in averaging the power density functions of the range gated signals. A frequency estimator is then used for estimating the central frequency of the signal peak. It is an estimate, \hat{f}_{het} , for the frequency, $f_{het} = \Delta f + f_t - f_{lor}$, of the heterodyne signal (see Figure 5.A.3).

Due to the analogue-to-digital conversion, the frequency interval resolved by the frequency analysis is limited to $(0, +F_s/2)$ or $(-F_s/2, +F_s/2)$ for complex valued signals. This limits the minimum and maximum values of \hat{f}_{het} and thus the interval of measurable radial velocities. As shown in reference [5], formula 5.A.5 estimates a range-gate average of the true wind radial velocity:

$$\hat{v}_r = -\frac{\lambda}{2} (\hat{f}_{het} - f_t + f_{lo})$$
(5.A.5)

For instance, in the case the signal is real valued (no complex-demodulation), the frequency offset $f_t - f_{lo}$ is set to about $F_s / 4$, so $|\hat{v}_r| \le \lambda F_s / 8$. Alternatively, a system specification requiring the possibility to measure radial winds up to v_{max} commands $F_s \ge 8v_{max} / \lambda$.

The averaging kernel is the convolution function between the pulse profile and the range-gate profile. Its length is a function of the pulse footprint in the atmosphere, Δr (see formula 5.A.6), of the range gate, Δx , and of the weighting factor, κ , where κ is the ratio between the gate full width at half maximum (FWHM) and Δx .

$$\Delta r = \frac{c \cdot T_{\rm p}}{2} \tag{5.A.6}$$

where:

 $T_{\rm p}$ is the FWHM duration of the laser pulse instantaneous intensity, g(t).

The range resolution, ΔR , is defined as the FWHM of the averaging kernel. For a Gaussian pulse and an unweighted range gate, ΔR is calculated according to formula 5.A.7^[6]:

$$\Delta R = \frac{c}{2} \cdot \frac{\Delta t}{\operatorname{erf}\left(\frac{\sqrt{\pi} \cdot \Delta t}{2T_{p}}\right)} = \frac{\Delta x}{\operatorname{erf}\left(\frac{\sqrt{\pi} \cdot \Delta x}{2\Delta r}\right)}$$
(5.A.7)

For a Gaussian pulse and a Gaussian weighted range gate, ΔR is equal to formula 5.A.8:

$$\Delta R = \frac{c}{2} \cdot \sqrt{T_{p}^{2} + (\kappa \cdot \Delta t)^{2}} = \sqrt{\Delta r^{2} + (\kappa \cdot \Delta x)^{2}} \quad (5.A.8)$$

ELEMENT 5: Floating object (Automatic) ELEMENT 6: Picture inline Element Image: 8_II_5-A3_en.eps END ELEMENT

Figure 5.A.3. Diagram showing how the frequency analysis is conducted

END ELEMENT

As shown in Figure 5.A.3, several signals are considered and range gated. The average spectrum is computed and a frequency estimator is applied.

Successive range gates can be partially overlapping (then successive radial velocity measurements are partially correlated), adjacent or disjoint (then there is a "hole" in the line-of-sight profile of the radial velocity).

Several possible frequency estimators are presented in reference [6] with a first analysis of their performances. Their performances are further discussed in reference [7]. Whatever the estimator, the probability density function of the estimates is the sum of a uniform distribution of "bad" estimates (gross errors) spread across the entire band $[-f_{max}, f_{max}]$ and a relatively narrow distribution of good estimates often modelled by a Gaussian distribution, as shown in formula 5.A.9:

$$p(\hat{f}_{het}) = \begin{cases} \frac{b}{2f_{max}} + \frac{1-b}{\sqrt{2\pi\sigma_f}} exp\left(-\frac{(\hat{f}_{het} - \bar{f}_{het})^2}{2\sigma_f^2}\right), for \ \hat{f}_r \in [-f_{max}, f_{max}] \\ 0 \ otherwise \end{cases}$$
(5.A.9)

In principle, the mean frequency, \overline{f}_{het} , can be different from the "true" heterodyne signal frequency, f_{het} . This can happen for instance when the frequency drifts during the laser pulse (chirp, see reference [8]). However, these conditions are rarely met and a good heterodyne Doppler lidar produces in practice unbiased measurements of Doppler shifts.

The parameter σ_f characterizes the frequency precision of the estimator. The corresponding radial velocity precision is $\sigma_V = \lambda \cdot \sigma_f / 2$. In a heterodyne system, it is typically of the order of several to several tens of centimetres per second. It degrades with the level of noise (power of n(t) in formula 5.A.3) and improves with the number of accumulated signals, *N*. In practice the improvement is limited as the accumulation of a large number of signals results in a long integration time during which the natural variability (turbulence) of the wind increases.

Reference [9] discusses the presence of gross errors (also called outliers^[1]) and proposes a model for the parameter b as a function of the several instrument characteristics and the level of detection noise. An outlier happens when the signal processor detects a noise peak instead of a signal peak. The parameter b is a decreasing function of the carrier-to-noise ratio. Quality checks must be implemented in heterodyne lidar systems so gross errors are filtered out and ignored as missing data. The presence of gross errors sets the maximum range of the lidar.

4.4 Target variables

The aim of heterodyne Doppler wind lidar measurements is to characterize the wind field. In each range interval, the evaluation of the measured variable leads to the radial velocity; see formula 5.A.5.

There are additional target values like the variability of the radial velocity that are not discussed in this annex.

The target variables can be used as input to different retrieval methods to derive meteorological products like the wind vector at a point or on a line (profile), in an arbitrary plane or in space as a whole. This also includes the measurement of wind shears, aircraft wake vortices (see figure in Attachment C), updraft and downdraft regions of the wind. An additional aim of the Doppler wind lidar measurements is to determine kinematic properties and parameters of inhomogeneous wind fields such as divergence and rotation. See examples of applications in Attachment C.

4.5 Sources of noise and uncertainties

4.5.1 Local oscillator shot noise

The shot noise is denoted n(t) in formula 5.A.3. Its variance is proportional to the local oscillator power, as shown in formula 5.A.10:

$$\left\langle n^2_{SN} \right\rangle = 2eSP_{\rm lo}B$$

(5.A.10)

where:

S is the detector sensitivity, $S = \frac{\eta e}{hf_{\star}}$, where η is the detector quantum efficiency;

B is the detection bandwidth.

It causes gross errors and limits the maximum range of the signal. If no other noise source prevails, the strength of the heterodyne signal relative to the level of noise is measured by the carrier-to-noise ratio (CNR), as shown in formula $5.A.11^{[6]}$:

$$CNR = \frac{\eta \cdot K \cdot \gamma(t)}{h \cdot f_t \cdot B} P_r(t)$$
(5.A.11)

Note: Some authors sometimes call "signal-to-noise ratio" what is defined here as the "carrier-to-noise ratio".

4.5.2 Detector noise

Additional technical sources of noise can affect the signal-to-noise ratio. As the shot noise, their spectral density is constant along the detection bandwidth (white noise).

(a) Dark noise is created by the fluctuations of the detector dark current, i_D , as shown in formula 5.A.12:

$$\left\langle n_{DN}^{2}\right\rangle = 2e\,i_{D}B\tag{5.A.12}$$

(b) Thermal noise (Johnson/Nyquist noise) is the electronic noise generated by the thermal agitation of the electrons inside the load resistor, R_L , at temperature T, as shown in formula 5.A.13:

$$\left\langle n^2_{TN} \right\rangle = \frac{4k_{\rm B}T}{R_{\rm L}} B$$
 (5.A.13)

where:

$k_{\rm B}$ is the Boltzmann constant.

4.5.3 Relative intensity noise

The relative intensity noise (dB/Hz) is the local oscillator power noise normalized to the average power level. The relative intensity noise (RIN) typically peaks at the relaxation oscillation frequency of the laser then falls off at higher frequencies until it converges to the shot noise level (pink noise). The RIN current increases with the square of the local oscillator power.

$$n_{\text{RIN}}^2 = (SP_{10})^2 10^{0.1\text{RIN}} B$$
 (5.A.14)

In a good lidar system, i_D , RIN, $1/R_L$ are low enough so that the local oscillator shot noise is the prevailing source of noise. In that case only, formula 5.A.14 is applicable.

4.5.4 Speckles

The heterodyne signal for a coherent Doppler wind lidar is the sum of many waves backscattered by individual aerosol particles. As the particles are randomly distributed along the beam in volumes much longer than the laser wavelength, the backscattered waves have a random phase when they reach the sensitive surface of the detector. They, thus, add randomly. As a result, the heterodyne signal has a random phase and amplitude. The phenomenon is called speckles (see reference [10]). It limits the precision of the frequency estimates.

4.5.5 Laser frequency

A precise measurement of the radial velocity requires an accurate knowledge of $f_r - f_{lo}$. Any uncertainty in this value results in a bias in \hat{f}_r . If the laser frequency, f_t , is not stable, it should either be measured or locked to f_{lo} .

4.6 Range assignment

The range assignment of Doppler measurements is based on the time elapsed since the emission of the laser pulse. This time must be measured with a good accuracy (the error, ε_t , must be smaller than or equal to $2\delta \cdot x / c$, where $\delta \cdot x$ is the required precision on the range assignment). This requires, in particular, that the time of the laser pulse emission is determined with at least this precision.

4.7 Known limitations

Doppler lidars rely on aerosol backscatter. Aerosols are mostly generated at ground and lifted up to higher altitudes by convection or turbulence. They are, therefore, in great quantities in the planetary boundary layer (typically 1 000 m thick during the day in tempered areas, 3 000 m in tropical regions), but in much lower concentrations above. It follows Doppler lidars hardly measure winds above the planetary boundary layer except in the presence of higher altitude aerosol layers like desert dusts or volcanic plumes.

Laser beams are strongly attenuated in fogs or in clouds. It follows the maximum range of Doppler lidars is strongly limited in fogs (a few hundreds of metres at best) and they cannot measure winds inside or beyond a cloud. They are able to penetrate into subvisible clouds as cirrus clouds. Therefore, wind information at high altitude (8 to 12 km) can be retrieved from crystal particle backscattering.

Doppler lidars detect cloud water droplets or ice crystals when they are present in the atmosphere. As they are efficient scatterers, they may dominate the return from the atmosphere, in case of heavy precipitation, for example, in which case the Doppler lidar measures the radial velocity of hydrometeors rather than the radial wind.

Rain downwashes the atmosphere, bringing aerosols to the ground. The range of a Doppler lidar is generally significantly reduced after a rain, before the aerosols are lifted again.

CHAPTER 5. SPECIAL PROFILING TECHNIQUES FOR THE BOUNDARY LAYER AND THE TROPOSPHERE

The presence of rainwater on the window of a Doppler lidar strongly attenuates its transmission. Unless a lidar is equipped with a wiper or a blower, its window should be wiped manually.

As explained in section 4.2, the efficiency of heterodyne detection is degraded by the presence of refractive index turbulence along the beam. Refractive index turbulence is mostly present near the surface during sunny days. The maximum range of Doppler lidar looking horizontally close to the surface may thus be substantially degraded in such conditions.

5. SYSTEM SPECIFICATIONS AND TESTS

5.1 System specifications

5.1.1 Transmitter characteristics

5.1.1.1 Laser wavelength

The laser wavelength depends mainly on the technology used to build the laser source. Most of the existing techniques use near-infrared wavelengths between 1.5 and 2.1 μ m, even though other wavelengths up to 10.6 μ m may be used. The choice of the wavelength takes into account the expected power parameters but also the atmospheric transmission and the laser safety (see references [11] and [12]). In fact, the choice of the window between 1.5 and 2.1 μ m is a compromise between technology and safety considerations (> 1.4 μ m to ensure eye safety).

5.1.1.2 Pulse duration

The laser pulse duration, T_p , is the FWHM of the laser pulse envelope, g(t). T_p defines the atmosphere probed length, R_p , contributing to the instantaneous lidar signal, as shown in formula 5.A.15:

$$R_{\rm p} = \frac{\rm c \cdot T_{\rm p}}{2}$$

(5.A.15)

As an example, a pulse duration of 200 ns corresponds to a probed length of approximately 30 m.

5.1.1.3 Velocity precision and range resolution vs. pulse duration

There is a critical relationship between the pulse duration and two performance-related features. A long pulse duration of several hundreds of nanoseconds leads to a potentially narrow FWHM of the laser pulse spectrum (if "chirping" can be avoided), (see the Fourier transform of the overall pulse in the time domain). This can lead to a very accurate wind measurement even for a very low signal-to-noise ratio provided that outliers can be avoided (see section 4.3). There is an adverse impact from high performance on range resolution. A pulse duration of 1 μ s limits the effective range resolution to approximately 150 m (see formula 5.A.6).

5.1.1.4 Pulse repetition frequency

The pulse repetition frequency, f_{PRF} , is the laser pulse emission frequency. f_{PRF} determines the number of pulses sent and averaged per line of sight in the measurement time. It also determines the maximum unambiguous range where the information of two consecutive sent laser pulses will not overlap. The maximum unambiguous range, R_{MaxO} , corresponds to f_{PRF} as in formula 5.A.16:

$$R_{\text{MaxO}} = \frac{c}{2f_{\text{PRF}_{\text{max}}}}$$
(5.A.16)

For example, for a maximum operational range of 15 km, the maximum f_{PRF} is 10 kHz.

As for radars, however, specific types of modulation (carrier frequency, repetition frequency, etc.) can overcome the range ambiguity beyond R_{MaxO} .

5.1.2 Transmitter/receiver characteristics

The transmitter/receiver is defined at least by the parameters given in Table 5.A.1.

Table 5.A.1. Transmitter/receiver characteristics

TABLE: Table horizontal lines

Transmitter/receiver characteristics	Remarks		
Aperture diameter	Physical size of the instrument's aperture that limits transmitted and received beams.		
Laser beam diameter and truncation factor	For a Gaussian beam, the laser beam diameter is defined as the diameter measured at $1/e^2$ in power at the lidar aperture. The laser beam diameter defines the illuminance level and so the eye safety. The truncation factor is the ratio between the diameter measured at $1/e^2$ and the physical size of the instrument's aperture.		
Focus point	Usually, pulsed lidars use collimated beams. For some applications, the beam can be partially focused at a given point to maximize the intensity on the beam laser within the measurement range. The intensity of the signal, and thus the velocity accuracy, will be optimized at this specific point.		

In principle, pulsed systems are monostatic systems. For continuous-wave systems, bistatic setups are also available.

5.1.3 Signal sampling parameters

The sampling of the pulsed lidar signal in range is determined by the parameters given in Table 5.A.2.

Table 5.A.2	Signal	sampling	parameters
-------------	--------	----------	------------

TABLE: Table horizontal lines	
Signal sampling parameters	Remarks
Range gating	The range gate positions can be defined along the line of sight.
Range gate width	Given by the sampling points or the sampling frequency of the digitizer. Should be chosen close to the pulse length.
Number of range gates	For real-time processing, spectral estimation of all range gates must be computed in a time less than the integration time.
Radial window velocity measurement range	Wind velocities as low as 0.1 m/s can be measured with the aid of Doppler wind lidar systems. The measurement range is restricted towards the upper limit only by the technical design, mainly by the detection bandwidth. A radial wind velocity range of more than 70 m/s can be measured.
Resolution of the radial velocity	The wind velocity resolution is the minimum detectable difference of the wind velocity in a time and range interval. A resolution of 0.1 m/s or better can be achieved by averaging.
5.1.4 Pointing system character	eristics

The pointing system characteristics are given in Table 5.A.3.

Table 5.A.3. Pointing system characteristics

Pointing system characteristics	Remarks
Azimuth range	When using a pointing device, a lidar has the capability to point its laser beam at various azimuth angles with a maximum angular capability of 2π . For endless steering equipment, a permanent steering along the vertical axis is allowed. Other scanning scenarios should be followed for non-endless rotation gear.
Elevation range	The pointing device can be equipped with a rotation capability around the horizontal axis. Potential 360° rotation can be addressed. Typical elevation angles are set from 0° to 180° in order to observe the semi-hemispherical part of the atmosphere above the lidar. Anyhow, a nadir pointing can be used for resting position of the equipment.
Angular velocity	The angular velocity is the speed at which a pointing device is rotating. A measurement can be performed during this rotation. In this case, the wind velocity information will be a mean of the various lines of sights in the probed area, between a starting angle and a stopping angle.
	Other scenarios of measurement can use a so-called step and stare strategy, with a fixed position during the measurement.
Angular acceleration	Defines how fast the angular velocity can change. To be defined for complex trajectories with fast changes in direction. Angle overshoots can be observed at high angular acceleration.
Pointing accuracy	The relative pointing accuracy is the standard deviation of the angular difference between the actual line-of-sight position (azimuth and elevation) and the position of the target (system of reference of the instrument).
	The absolute pointing accuracy needs prior calibration by angular sensors (pitch, roll, heading) (system of geographical reference).
Angular resolution	Minimum angle step that the line of sight can move. It can be limited by a motor reduction factor, position, encoder or mechanical friction.

5.2 Relationship between system characteristics and performance

5.2.1 Figure of merit

A figure of merit (FOM) helps to compare range performance of different lidars with different parameters. The example shown in Figure 5.A.4 allows the classification of pulsed lidar sensitivities, independently of atmospheric parameters. FOM is derived from the lidar equation (see formula 5.A.4) and is proportional to velocity spectrum, CNR, which is defined on the averaged spectral density as the Doppler peak intensity divided by the spectral noise standard deviation, assumed to be constant (white noise). *N* is the number of averaged pulses.

FOM is defined for a set of lidar parameters as in formula 5.A.17:

$$FOM = \eta_{all} \cdot E \cdot T_p \cdot D^2 \cdot \sqrt{t_i \cdot f_{PRF}}$$
 (5.A.17)

where:

- $\eta_{\rm all}$ is the overall efficiency, taking into account beam and image quality, overall transmission and truncation factor;
- *E* is the laser energy at the laser output (received energy is proportional to peak power and laser footprint);
- T_{p} is the pulse duration (this term comes from narrow bandwidth, inversely proportional to T_{p});

- *D* is the collecting telescope diameter (for typical long-range applications, the optimum is 100 to 150 mm in size for near-infrared wavelengths);
- t_i is the integration time for one line of sight;

 f_{PRF} is the pulse repetition frequency.

The FOM is proportional to the square root of number N of accumulated spectra: $N = t_i \cdot f_{PRF}$.

When comparing two lidars at two different wavelengths, spectral dependence of atmospheric parameters should be considered. The FOM must be calculated with an integration time less than or equal to 1 s to avoid that wind or turbulence may fluctuate more than the Doppler spectral width.

A lidar may increase its FOM with a longer accumulation time within this 1 s time limit.

Considering state-of-the-art low aberration optical components, η_{all} can be estimated by the product of the emitting path transmission and the receiving path transmission.

It has to be noted that the FOM for a pulsed Doppler lidar may not be increased indefinitely by increasing the collecting area, D^2 , since phase distortion across the beam due to refractive index turbulence degrades the heterodyne efficiency^[3]. A practical limit is in the vicinity of a D = 125 mm useable diameter for long-range lidars.

Since the velocity spectrum CNR is inversely proportional to the squared range, the maximum operational range is approximately proportional to the square root of FOM, when atmospheric absorption can be neglected. When FOM is expressed in mJ ns m², the maximum operational range, expressed in km, is almost the square root of FOM.

ELEMENT 7: Picture inline fix size Element Image: 8_II_5-A4_en.eps END ELEMENT

Figure 5.A.4. Example of a figure of merit

Table 5.A.4 computes the FOM for typical lidar figures and their corresponding typical measurement range.

 Table 5.A.4. Figure of merit for typical lidar figures and their corresponding typical measurement range

TABLE:	: Table horiz	ontal lines					
η	E (<i>mJ</i>)	T _p (ns)	D(<i>m</i>)	f _{PRF} (Hz)	t _i (s)	FOM (mJ ns m²)	Typical measurement range (km)
0.5	0.2	800	0.12	10 000	1	115	10
0.5	0.1	400	0.06	20 000	1	10	3
0.5	2	300	0.12	750	1	118	10

5.2.2 Time-bandwidth trade-offs

A good practice is to match the pulse duration with the desired range gate (see section 4.6) so that the spatial resolution depends equally on these two parameters. With this assumption, spatial resolution is proportional to pulse duration. The shorter the pulse, the better the resolution. Velocity resolution is proportional to spectrum width and is larger when the spectrum is narrow. Because the spectrum width is inversely proportional to the pulse duration, range resolution and velocity resolution are also inversely proportional.

5.3 **Precision and availability of measurements**

5.3.1 Radial velocity measurement accuracy

Radial velocity measurement accuracy is defined (according to ISO 5725-1) in terms of:

- (a) Trueness (or bias) as the statistical mean difference between a large number of measurements and the true value;
- (b) Precision (or uncertainty) as the statistical standard deviation of a series of independent measurements. It does not relate to the true value.

Lidar data of good quality are obtained when the precision of the radial velocity measurements is higher than a target value (for example 1 m/s) with a predefined probability of occurrence (for example 95_%).

An error value (1_{σ}) of 0.5 m/s can be regarded as adequate for typical meteorological applications and for wind measurements to determine the statistics of dispersion categories for air pollution modelling^[13]. For wind energy applications, the requirements may be higher (0.2 m/s).

5.3.2 Data availability

Data availability is defined as the ratio of data with precision, *P*, to the total number of data during a measurement period.

The availability of measurement data, that is, the determinability of the wind profile, is a function mainly of the aerosol concentration and the clouds. Other filtering criteria may be applied, depending on the required data accuracy. For example, data that exhibit significantly non-uniform flow around the scan disk should be rejected.

5.3.3 Maximum operational range

Assuming the lidar line of sight remains within the planetary boundary layer (that is, no significant change of signal along the line of sight), Figure 5.A.5 shows a typical pulsed lidar data availability versus range plot.

ELEMENT 8: Floating object (Bottom) ELEMENT 9: Picture inline fix size Element Image: 8_II_5-A5_en.eps END ELEMENT

Figure 5.A.5. Example for maximum operational range

END ELEMENT

In this case, the range for 80_% data availability (P_{80}) is 7 500 m.

The performance shown in this diagram is based on a standard atmosphere:

- (a) No clouds along the line of sight;
- (b) No precipitation;
- (c) Visibility over 10 km (clear air).

This performance will vary significantly with relevant local climatic and operational conditions. Data from greater ranges should be treated with caution, depending on the application.

Measurement range must be defined with a given availability criteria. A recent study about this link is described in reference [14].

For example, R_{50} corresponds to the maximum range with availability over 50_%.

If the availability is not mentioned, the maximum operational range is supposed to be R_{80} , that is, the maximum distance where the availability is over 80_%.

For a given availability, a change in velocity precision leads to a change in maximum operational range.

5.4 Testing procedures

5.4.1 General

In order to accurately assess for the accuracy of the target variables, the manufacturer should perform a set of validation tests for the range and velocity. Some can be performed under laboratory conditions. Certain other validation tests can only be performed by a comparison with other reference instruments, such as cup or sonic anemometers.

5.4.2 Radial velocity measurement validation

5.4.2.1 General

This section describes how the quality of radial velocity measurements can be checked and assessed.

5.4.2.2 Hard target return

This test consists in acquiring wind measurements with the beam directed to a stationary (unmoving) hard target (any building within lidar range) and checking the radial velocity measurement returned by the lidar is 0 m/s.

This test checks that the frequency difference, $f_t - f_{lo}$, between emitted laser pulses and the local oscillator is known or determined with a sufficient accuracy (see section 4.5.3).

The range gate length should be close to the length of the laser pulse, and the distances of the range gates should be set so that the hard target is exactly at the centre of one range gate, otherwise, a velocity bias can occur in case of frequency drift within the pulse.

Hard target velocity measurements should be acquired during at least 10 min. The test is successful if the time sequence of hard target radial velocities is centred at about 0 m/s.

5.4.2.3 Self-assessment of radial velocity precision

In this test, the pulsed lidar beam is vertical and radial velocity measurements are acquired during at least 20 min at the rate of at least one profile of radial velocities every second. Let us denote by $v_r(x,k)$, k = 1,...,K the time sequence of radial velocities measured at distance x. The test consists in forming the power spectrum of the time sequence, as shown in formula 5.A.18:

$$V(x,f) = \frac{1}{K} \left| \sum_{k=1}^{K} v_r(x,k) \exp\left(-2j\pi f k \delta t\right) \right|^2 \quad (5.A.18)$$

where:

 δt is the constant time lag between successive $v_r(x,k)$ measurements.

On average, the power spectrum V(x, f) should look like Figure 5.A.6. At low frequencies, the power spectrum is dominated by natural wind fluctuations and will follow a $f^{-5/3}$ law. At high frequencies, the power spectrum is dominated by the flat level of measurement errors (white noise). The level of this flat part directly gives the variance of these measurements $\sigma_e^2(x)$.

Note: The test must be carried out at night when the natural variability of the wind is weak, that is, when the wind is considered to be calm. It may then happen that measurement errors are much larger than natural wind fluctuations so the $f^{-5/3}$ part of the power spectrum is hidden.

Fully described in reference [15], this technique allows for the estimation of the measurement precision of the lidar without any ancillary data.

ELEMENT 10: Floating object (Automatic) ELEMENT 11: Picture inline fix size Element Image: 8_II_5-A6_en.eps END ELEMENT

Figure 5.A.6. Power spectrum of radial velocity measurements

END ELEMENT

In Figure 5.A.6, the line is V(f). At low frequencies, V(f) should be proportional to $f^{5/3}$ (spectral behaviour of natural wind variability; see dashes). At high frequencies, the spectrum becomes flat (dash-dot line) at a level directly equal to the variance of measurement errors, $\sigma_e^2(x)$.

5.4.3 Assessment of accuracy by intercomparison with other instrumentation

5.4.3.1 Sonic anemometer

The last test consists of directing the lidar beam very close to a sonic anemometer on a mast or platform without vibration and comparing lidar radial velocities with the projection of the threedimensional wind vectors acquired by the sonic anemometer on the beam direction.

Lidar and sonic anemometer data must be averaged over a minute.

The direction of the lidar beam must be determined with a good accuracy (of the order 1° or better) and as close as possible to the horizontal plane. The lidar beam must be at the height of the sonic anemometer (height difference of the order of 1 m or less).

The root mean square of the differences between lidar and sonic anemometer data must be less than 0.1 m/s.

The mast will most likely cause wind flow perturbations downstream. Winds coming from directions such that the sonic anemometer is in the perturbed zone must be removed from the statistics.

5.4.3.2 Performance test against masts

The mast must be equipped with at least three-cup anemometers mounted horizontally.

5.4.3.3 Comparison with Doppler weather radars

The possibility for intercomparison between Doppler lidars and Doppler weather radars can be an option where the two systems are collocated. The details about this class of intercomparison are just becoming known as the deployment of systems integrating both sensors for all-weather remotesensing of the wind field at airports, especially for wind shear detection, is just getting under way. Studies have recently been conducted^[16;17;18]. Both sensors should be collocated and should probe the same atmospheric volume in order to be certain of representative intercomparisons.

In addition to the siting requirement, it is very important that weather situations be selected in which the tracer targets of both sensors actually represent the flow of air. In conditions of dry weather, the Doppler lidar works best, while under such conditions of clear air, the radar measures only the returns due to scattering by insects. These scattered signals from insects provide no accurate indication of the actual air movement. Comparison with data from Doppler lidars typically shows differences of up to several metres per second. Therefore, echo classification in terms of radar targets has to be enabled in order to be able to reject insect returns. This means that the radar has to be capable of measuring at two orthogonal linear polarizations. During precipitation events, however, conditions are optimal for the radar, whereas the lidar may have significantly reduced range coverage. In weather situations with light rain or drizzle from stratiform cloud, both radar and lidar sensors are expected to obtain high-quality data. Such situations are thus best suited for this validation procedure. Appropriate filtering of radar data on the basis of target classification

using dual-polarization moments needs to be conducted in order to get rid of any nonmeteorological returns.

If these requirements are fulfilled, cross-comparison of Doppler weather radar and Doppler lidar can be performed on the basis of profiles of horizontal wind as obtained, for example, with velocity volume processing or velocity azimuth display methods. In this case, the scan geometry has to be considered. Ideally, the scan geometry for the radar and lidar should be the same with respect to elevation angles. Another option yet to be evaluated could be to compare the actual radial wind velocities on a range gate by range gate basis between the radar and lidar systems.

5.4.3.4 Comparison with radar wind profilers

Comparison with radar wind profilers may be performed if the two systems are collocated. The weather conditions under which both sensors work optimally are not exclusive of each other (sufficient aerosol tracers for lidar and sufficient turbulent eddies as targets for Bragg scattering for the wind profiler). Care must be taken that both sensors face optimal atmospheric conditions. Additionally, attention has to be paid to the scan mode used to derive the vertical wind profile so that the volume probed by the lidar matches the volume probed by the wind profiler.

5.4.4 Maximum operational range validation

In clear sky conditions, the atmosphere can be described by the visibility, V, the aerosol concentration and the aerosol type, where the last two can be properly described by the two optical lidar parameters extinction and backscatter coefficients. The visibility (see, for example, ISO 28902-1) and humidity are measured by standard ground-based meteorological local sensors, whereas the aerosol type and its size distribution are not. To simplify, atmosphere types can be sorted in a few categories associated with their lidar ratio. Lidar ratio values in the near infrared typically are limited in the range of 30 to 50 steradians. R_{MaxO} will not be too dependent on the aerosol variability on site except for conditions with local pollution sources.

Visibility is an important parameter for lidar range. The lidar equation (see formula 5.A.4) indicates that the received power is proportional to the backscatter coefficient and decreases exponentially with extinction, thus increases with visibility. Since α (x) and β (x) are proportional, there is a maximum to the function $P_r(t)$ (see lidar equation in formula 5.A.4, and Figure 5.A.7), and so for R_{MaxO} .

To discard unfavourable visibility conditions for coherent Doppler wind lidars (fog and very clear), only haze and clear visibility conditions are selected for range measurements. Current lidars can work in precipitating conditions, but are subject to error in their determination of the vertical wind component; the horizontal component has been shown to be very accurate (see reference [18]).

ELEMENT 12: Picture inline	
Element Image: 8_II_5-A7_en.eps	
END ELEMENT	

Figure 5.A.7. Dependency of the maximum operational range of the heterodyne Doppler signal to the visibility conditions

Table 5.A.5. Plot numbers

TABLE: Table horizontal lines

Plot number	1	2	3	4	5
Typical FOM for 1 s integration time (mJ ns m ²)	20	30	60	100	150

Because backscatter changes rapidly for high relative-humidity values, data corresponding to relative humidity $> 70_{\%}$ should be filtered out the measurement dataset. So, precipitation conditions (rain, snow) are not considered.

Moreover, index turbulence, Cn^2 (depends on temperature and altitude), can modify R_{MaxO} by altering the beam wave front. Strong turbulent conditions must be removed from datasets (sunny days around noon), and experimental protocol must be followed up.

So the validation must be conducted under the following conditions:

- (a) The lidar is operated in operational conditions (vertical for profilers, low elevation for scanning lidars);
- (b) The full measurement range remains in the boundary layer;
- (c) 10 km < visibility < 50 km (at visible wavelength, dependency with wavelength is given in ISO 28902-1);
- (d) No precipitation;
- (e) No cloud on the line of sight;
- (f) $Cn^2 < 10^{-14} m^{-2/3}$ (1 m above ground level).

Data not corresponding to these conditions should be filtered out for assessing the maximum operational range.

- (a) Context conditions are recorded simultaneously (temperature, Cn², visibility, relative humidity);
- (b) Datasets are created following the above-mentioned atmospheric conditions. 100 h of filtered data are required as a minimum for a good statistical dataset. It represents around four days of cumulated measurements with 1 s accumulation time. Depending on the atmospheric conditions, the evaluation period can last from four days and up to one month.

6. MEASUREMENT PLANNING AND INSTALLATION INSTRUCTIONS

6.1 Site requirements

The selection of the measurement site is essentially determined by the measurement task. Careful selection of the measurement site is necessary, in particular, for stationary systems or for the quasistationary use of mobile systems during long-term measurement campaigns. The following points must be taken into account when selecting the measurement site:

- (a) Unobstructed view: Unrestricted visibility can be limited by built-up areas, trees and buildings near the installation site of the lidar. If the view is limited by buildings, it is possible to avoid the limitation of the horizontal view by selecting a larger elevation angle. In the case of a velocity azimuth display scan, the measurement signals originating not from the free atmosphere but from obstacles must be excluded from the evaluation;
- (b) Electromagnetic radiation: Doppler wind lidar systems should be shielded properly against interferences by electromagnetic radiation (for example by radar, mobile radio or cellular phone networks).

Early inspection of the envisaged measurement site with the participation of experts (such as meteorologists) is recommended.

For optimal operational range retrieval, the lidar should be installed on a short grass-covered ground with no nearby structures, which would cause atmospheric turbulence affecting the lidar's operation and performance. The lidar should be installed at least at 3 m above the ground, especially when not located on a grass ground, like concrete, asphalt or a plain metallic platform, in order to avoid

effects from turbulence nearby the optical output that will destroy the coherency of the atmosphere and thus drastically diminish the detection.

6.2 Limiting conditions for general operation

Interference factors regarding Doppler wind lidar measurements are:

- (a) Optically thick clouds;
- (b) Precipitation of any type (rain, hail, snow);
- (c) Blocking effects (such as from buildings).

6.3 Maintenance and operational test

6.3.1 General

To ensure the system functions as specified and to rule out deviations and technical errors such as maladjustments^[19], maintenance and operational tests must be performed in regular intervals. In addition to the information given here, typical application ranges and corresponding requirements can be found in Attachment D.

6.3.2 Maintenance

Maintenance such as regular cleaning of the optical components, calibration, etc. must be performed as a basic requirement of quality assurance. Maintenance procedures may be conducted by on-site personnel, using an automatic software detection of the decrease of the signal due to, for example, dust deposits, and making appropriate corrections to the data, or a combination of the two. Typical maintenance intervals are three months depending on the environmental conditions.

6.3.3 Operational test

Operational tests should be performed every 6 to 36 months. The tests depend on the individual system design. The manufacturer must specify the testing procedures and provide the necessary testing tools.

- (a) Output power and frequency of the laser source should be measured at the periodicity indicated by the manufacturer;
- (b) Signal output of the data acquisition system reacting to a defined light pulse or defined target should be measured at the periodicity indicated by the manufacturer;
- (c) For scanning or steering systems, an alignment test using a calibrated instrument (for example a compass or inclination meter) should be performed.

6.3.4 Uncertainty

Table 5.A.6 compiles uncertainty contributions to the measurement variables and the line-of-sight wind velocity. The uncertainty contributions of the measurement variables influence the quality of the data produced by the system. The dominant uncertainties result from:

- (a) The initial calibration process of the system by the manufacturer;
- (b) The prevailing environmental conditions.

Table 5.A.6. Effects leading to uncertainty

 TABLE: Table horizontal lines

Measurement variables

Effects leading to uncertainty

Measurement variables	Effects leading to uncertainty		
Signal-to-noise ratio	(a) Noise including detector noise		
	(b) Speckle effect (when only a few pulses are averaged during the measurement time)		
	(c) Laser power or pulse width fluctuations		
	(d) Refractive index (temperature) turbulence		
	(e) Lag angle at fast rotation speeds		
Frequency shift, Δf	(a) Bias and fluctuations of emitted pulse frequency compared to local oscillator frequency		
	(b) Pulse length		
	(c) Signal-to-noise ratio		
	(d) Number of averaged pulses		
	(e) Quality of estimator		
Target variable	Uncertainty contribution		
Line-of-sight wind velocity	(a) Wind turbulence		
(radial wind velocity)	(b) Wind gradient along the line of sight		
	(c) Hard targets close to the range gate		

SECTION: Chapter_book Chapter title in running head: CHAPTER 5. SPECIAL PROFILING TECHNIQUES... Chapter_ID: 8_II_5_annex_en Part title in running head: PART II. OBSERVING SYSTEMS

ATTACHMENT A. CONTINUOUS-WAVE DOPPLER WIND LIDAR

(informative)

As stated in this annex, there are several methods by which lidar can be used to measure atmospheric wind. The four most commonly used methods are pulsed and continuous-wave coherent Doppler wind lidar, direct-detection Doppler wind lidar and resonance Doppler wind lidar (most commonly used for mesospheric sodium layer measurements).

This annex describes the use of heterodyne (coherent) pulsed lidar systems. It should be noted that there is also ISO 28902-3 currently in preparation, which describes the use of continuous-wave coherent Doppler wind lidar for the measurement of atmospheric wind. ISO 28902-3 will specify the requirements and performance test procedures for continuous-wave Doppler lidar techniques and present their advantages and limitations. The term "continuous-wave Doppler lidar" or "continuous-wave Doppler wind lidar" is used in this annex to apply to continuous-wave lidar systems making measurements of wind characteristics from the scattering of laser light by aerosols in the atmosphere within the low-altitude boundary layer. A description is provided of typical measurement geometries, signal-processing options, performance requirements, and limits based on standard atmospheric conditions. The applications for continuous-wave lidar are, among others:

(a) Wind energy;

- (b) Wind resource assessment;
- (c) Power curve verification;
- (d) Loss factor in the wind farm operation;
- (e) Wind hazards monitoring for aviation weather applications;
- (f) Wind shear;
- (g) Requirements for the detection of wake vortices behind aircraft.

ISO 28902-3 will address manufacturers of continuous-wave Doppler wind lidars, as well as those bodies concerned with testing and certifying their conformity. It will also provide recommendations for users to make adequate appropriate use of these instruments. A comprehensive bibliography of independent publications will be provided.

SECTION: Chapter_book Chapter title in running head: CHAPTER 5. SPECIAL PROFILING TECHNIQUES... Chapter_ID: 8_II_5_annex_en Part title in running head: PART II. OBSERVING SYSTEMS

ATTACHMENT B. RETRIEVAL OF THE WIND VECTOR

(informative)

B.1 General

The wind is a three-dimensional vector quantity, with the wind field being generally a function of space and time. The measurement of the instantaneous wind at a particular position therefore always requires the determination of three vector components. A single Doppler lidar is only able to measure the component (or projection) of the wind vector along the line of sight of the laser beam. Three separated lidar systems would therefore be required to perform an exact local measurement at any fixed time. Under certain assumptions, it is possible to estimate the full wind vector from a single "monostatic" Doppler lidar. This process is called wind retrieval since the accuracy of the wind vector estimate depends on the validity of the assumptions regarding the wind field.

B.2 Coordinate system

The figure below shows the wind vector $\vec{u}(\vec{r},t)$ in the Cartesian coordinate system with the unit vectors $\vec{\iota}_i \vec{j}_i \vec{k}$. The components u_x , u_y , u_z are scalar functions of position, and time, $\vec{r} = \vec{r}(x, y, z, t)$, is the position or radius vector of an air parcel.

$$\vec{u} = \frac{d\vec{r}}{dt} = \begin{pmatrix} u_x \\ u_y \\ u_z \end{pmatrix}$$
(B.1)

or

$$\vec{u} = \left[u_x \cdot \vec{i} + u_y \cdot \vec{j} + u_z \cdot \vec{k}\right]$$
(B.2)

The coordinate system in the figure points to the east (E) with the positive x-direction (\vec{i}) , to the north (N) with the positive y-direction (\vec{j}) and to the zenith with the positive z-direction (\vec{k}) .

Coordinate system and wind vectors

With θ and ϕ , the components in Cartesian coordinates are:

$$\begin{split} u_{\rm x} &= U \cdot \cos \phi \cdot \sin \theta \\ u_{\rm y} &= U \cdot \cos \phi \cdot \cos \theta \\ u_{\rm z} &= U \cdot \sin \phi \end{split}$$

and the three-dimensional wind vector becomes:

$$\vec{u} = \begin{pmatrix} U \cdot \cos \phi \cdot \sin \theta \\ U \cdot \cos \phi \cdot \cos \theta \\ U \cdot \sin \phi \end{pmatrix}$$

Example: Horizontal west wind: $\theta = 90^{\circ}$, $\varphi = 0^{\circ}$

$$\Rightarrow u_x = U, \ u_y = u_z = 0 \implies \vec{u} = (U, 0, 0)$$

B.3 Horizontal wind vector

The horizontal wind vector, \vec{u}_h , and the horizontal projection of the three-dimensional wind vector, \vec{u} , in the figure becomes:

$$\vec{u}_h = \begin{pmatrix} u_x \\ u_y \end{pmatrix} = \begin{pmatrix} u_h \sin \theta \\ u_h \cos \theta \end{pmatrix}$$
(B.5)

(B.3)

or, in component notation:

$$u_h = |\vec{u}_h| = U \cdot \cos \phi = \sqrt{u_x^2 + u_y^2}$$
 (B.6)

The value u_h is denoted as horizontal wind velocity or colloquially as wind velocity. According to the meteorological convention, the wind direction is defined as the direction opposite to the wind vector, \vec{u}_h . It is oriented clockwise from north via east, south and west (see figure above).

For the case of a lidar scanning in a disk at fixed elevation angle in uniform wind flow, the individual line-of-sight velocity points follow a cosine form as a function of azimuth angle. The peaks of the function correspond to the azimuth angle aligned parallel or anti-parallel to the wind direction. The function passes through zero when the azimuth angle is perpendicular to wind bearing since there is no component of velocity along the line of sight. The data are also conveniently displayed on a polar plot, which provides information at a glance on the speed, direction and vertical wind component. A standard least-squares fitting routine provides the best estimates of the values of the three unknown parameters (either *u*, *v* and *w*, or alternatively, horizontal speed, vertical speed and wind bearing).

B.4 Radial velocity

In lidar measurements, the component v_r of the local wind vector $\vec{u}(\vec{r},t)$ in the beam direction of the laser, i.e. the radial velocity at any arbitrary position \vec{r} , is the direct measurand determined from the Doppler frequency shift (see Figure 5.A.5). If the wind vector $\vec{u}(\vec{r})$ is written in a spherical coordinate system $(\vec{e}_r, \vec{e}_\theta, \vec{e}_\phi)$ instead of a Cartesian $(\vec{t}, \vec{j}, \vec{k})$ coordinate system, the radial velocity, v_r , is easily defined (compare formula B.2)^[20]:

$$\vec{u}(\vec{r}) = \vec{u}(r,\theta,\phi) = \left[u_r \cdot \vec{e}_r + u_\theta \cdot \vec{e}_\theta + u_\phi \cdot \vec{e}_\phi\right]$$
(B.7)

where:

 \vec{e}_r is the unit vector in the beam direction;

 $\vec{e}_{\theta}, \vec{e}_{\phi}$ are the unit vectors in the azimuth and elevation direction;

 $u_{r}, u_{\theta}, u_{\phi}$ are the orthogonal wind vector components of the coordinate system carried along during the scanning operation.

The projection of the wind vector $\vec{u}(\vec{r})$ onto the beam direction, i.e. the scalar product (•), can be derived with formula B.8:

$$\vec{u}(\vec{r}) \circ \vec{e}_r = u_r \equiv v_r \equiv -v_{LOS} \tag{B.8}$$

 v_{LOS} is equal by convention to the negative radial component v_{r} of the local wind vector at the position \vec{r} . The negative sign of v_{LOS} corresponds to the convention that in lidar systems the wind velocity is regarded as positive towards the laser.

With the known transformation relation between spherical and Cartesian coordinates^[19], v_r can be expressed by the Cartesian wind components u_{xr} , u_{yr} , u_z the result being:

$$v_{\text{LOS}} = -v_{\text{r}} = -\left(u_{\text{x}} \cdot \cos\phi \cdot \sin\theta + u_{\text{y}} \cdot \cos\phi \cdot \cos\theta + u_{\text{z}} \cdot \sin\phi\right) (B.9)$$

B.5 Retrieval of the wind vector

The atmosphere should be sensed at different angles in order to detect the (Cartesian) components u_x , u_y , u_z of the wind vector with the Doppler wind lidar.

Note: The wind components u_x , u_y , u_z are frequently also called u, v, w.

However, all wind components are usually subject to spatial and temporal fluctuations since the wind field in general cannot be regarded as homogeneous and stationary due to a variety of small-scale atmospheric processes like gravity waves, convection, turbulence or orographically induced flow effects. Homogeneity assumptions should therefore be made in order to retrieve an estimate of the wind vector from the radial components. The better this assumption holds, the more does the estimate represent the actual wind field. The problem has been extensively discussed in the literature and is explained in textbooks for both radar and lidar, see, for example, references [21] and [22].

Therefore, assuring that the wind field can be regarded as stationary over the measurement period and horizontally homogeneous over the sampled volume, that is, if the wind field is only a function of the vertical coordinate z, then the radial wind measurements for a fixed geometrical height are given by formula B.10, the simple matrix equation:

 $A \cdot u = v_{\rm r} \tag{B.10}$

The rows of this $(n \ge 3)$ matrix A are comprised of the unit directional vectors describing the pointing of the n beams. The vector v_r is also of dimension n and contains the radial winds obtained in the n pointing directions. This is nothing more than a compact notation for the n scalar (inner) products as given in formula B.8. For n = 3, the inverse A^{-1} exists if A has rank 3 (for example, all row vectors are linearly independent) and the wind vector can be directly obtained through formula B.11:

$$u = A^{-1} \cdot v_{\rm r} \tag{B.11}$$

For n > 3 and rank(A) = 3, the linear system is overdetermined and has usually either one solution or no (exact solution) at all. However, an approximate solution can be found which minimizes $||A \cdot u - v_r||^2$. This least-square solution can be expressed by the Pseudoinverse $(A^TA)^{-1} \cdot A^T$ of matrix A as shown in formula B.12:

$$u = \left(A^{\mathrm{T}}A\right)^{-1} \cdot A^{\mathrm{T}} \cdot v_{\mathrm{r}} \tag{B.12}$$

CHAPTER 5. SPECIAL PROFILING TECHNIQUES FOR THE BOUNDARY LAYER AND THE TROPOSPHERE

 A^{T} denotes the transpose of matrix A. Formula B.12 is sufficiently general and describes all possible scanning configurations with n discrete beam pointing directions. Care must be taken in the practical use of this formula to obtain numerically stable implementations.

The Doppler beam swinging technique or the velocity azimuth display scanning methods are two frequently used scan schemes for Doppler lidars.

In the case of the Doppler beam swinging technique, measurements are performed in at least three linearly independent directions. This method allows for a very fast scanning, but it may yield biased measurements if the wind field is non-homogeneous. The validity of the retrieval assumptions (homogeneity, stationarity) can be tested to some extent if more than three directions are used. An explicit example of the Doppler beam swinging method with n = 3 and n = 4 can be found in reference [23].

In the case of the velocity azimuth display scan, the beam direction azimuth is varied in a continuous scanning operation. The variation of the azimuth angle during the measurement series yields a set of different projections of the local wind vector onto these measurement directions. The elevation angle remains constant in the process. Originally, the velocity azimuth display method was proposed for a horizontally homogeneous wind field^[24]. Later discussions were extended to allow for an additional linear variation of the vector components^[25]. In the case of a homogeneous wind field, the result is a sinusoidal profile of the measured velocity v_{LOS} .

If the lidar is powerful enough to provide several azimuth scans at different elevations in reasonable time, these can be combined in order to compile a full volume scan. This makes it feasible to use a more elaborate model of the wind field that can be fitted to the vector of observations of v_r . That is, analogous to formula B.10, one can further expand the Taylor series incorporating also shearing of the wind, i.e. the first spatial derivatives. For Doppler radars, this procedure is standard and is commonly known as velocity volume processing. It has been originally published in reference [26]. This analysis then leads to formula B.13 instead of formula B.10:

$$v_{r} = \sin\theta \cdot \cos\phi \cdot u_{0} + \cos\theta \cdot \cos\phi \cdot v_{0} + \sin\phi \cdot w_{0}$$

+ $r \cdot \sin^{2}\theta \cdot \cos^{2}\phi \cdot u'_{x}$
+ $r \cdot \cos^{2}\theta \cdot \cos^{2}\phi \cdot v'_{y}$
+ $r \cdot \cos\theta \cdot \sin\theta \cdot \cos^{2}\phi \cdot (u'_{y} + v'_{x})$ (B.13)
+ $\sin\phi \cdot (r \cdot \sin\phi - z_{0}) \cdot w'_{z}$
+ $\sin\theta \cdot \cos\phi \cdot (r \cdot \sin\phi - z_{0}) \cdot (u'_{z} + w'_{x})$
+ $\cos\theta \cdot \cos\phi \cdot (r \cdot \sin\phi - z_{0}) \cdot (v'_{z} + w'_{y})$

It should be noted that this model does not allow to extract any information about horizontal vorticity since u'_{x} and v'_{x} only appear as a sum in formula B.13. This method has been applied to lidar data and compared with Doppler weather radar data in reference [16].

SECTION: Chapter_book Chapter title in running head: CHAPTER 5. SPECIAL PROFILING TECHNIQUES... Chapter_ID: 8_II_5_annex_en Part title in running head: PART II. OBSERVING SYSTEMS

ATTACHMENT C. APPLICATIONS

(informative)

C.1 Wind energy

C.1.1 General

One of the main challenges in the wind energy market today is the optimal estimation of the future electrical output of a wind farm. Today, the procedure to estimate this is to have the best evaluation possible of the wind potential at a given site, the best evaluation of what a wind turbine can produce with the free wind that it receives and to properly evaluate the total production loss that can occur during the wind farm operation. Some of these losses can be due to the wakes, to the power performance loss of a wind turbine, downtime due to operation and maintenance of the wind farm and other parameters that can affect the global wind farm operation. Today, the ground-based coherent Doppler lidar is a suitable tool to be used during all the phases of the operation of a wind farm, from the development phase, to the commissioning, operation and repowering of old wind farms.

C.1.2 Wind resource assessment

Today the ground-based vertical-profiler lidar (both pulsed and continuous-wave types) is widely used in the wind energy market by all major developers in order to provide highly accurate wind speed data and reduce the horizontal and vertical uncertainty during the wind resource assessment campaign. Today ground-based coherent Doppler lidar can be used without any mast during the campaign and these data are considered as bankable. Considering the size of the wind turbine and the height that it can reach, the lidar allows a proper evaluation of the vertical wind profile that is critical for the design of a wind turbine. The vertical wind shear (change in wind speed along the vertical axis) and the vertical wind veer (change in wind direction along the vertical axis) are two key elements to be considered that can affect the annual energy production of a wind farm.

The wind farms are moving more and more offshore, and today the ground-based pulsed-scanning lidar can be used for wind resource assessment campaign scanning offshore from the shore. This allows to decrease the horizontal uncertainty in the wind resource assessment campaign at a much reduced cost than the standard offshore met mast. In addition to this, the correlation of the wind measured with the scanning lidar can be used to validate some wind models for the wind transition offshore to the shore.

C.1.3 Power curve verification

C.1.3.1 General

Today, the International Electrotechnical Commission (IEC) standard 61400-12-1^[27] mentions that a met mast is to be used for the power curve verification of a wind turbine. Considering the maturity of the ground-based lidar for the wind resource assessment application, IEC 61400-12-1 is in the process of evolving and will be including the ground-based lidar vertical profiler for power curve verification.

The power curve verification standard is also including a new measurement method by applying the rotor equivalent power curve. In this case, the entire wind profile of the rotor diameter is considered and used, in order to estimate the total incoming wind along a plane rather than only the wind coming at hub height.

In addition to the vertical profiler, when a wind turbine cannot be reached within the 2.5D distance of the free wind of the wind turbine (where D is the rotor diameter), the scanning ground-based lidar can also be used to perform some power curve verification, by scanning from the ground to the front of the wind turbine.

C.1.3.2 Loss factor in the wind farm operation

When globally looking at a wind farm, there are some loss coefficients that wind farm developers apply to their annual electrical production output calculation, and the more accurate this information, the better the project and ease of financing.

The ground-based lidar is being used in a variety of programmes for the validation of the wake loss deficit coefficient. Major wind farm developers/owners have their own wind flow modelling tool to

I

optimize the wind farm design and layout, and today the ground-based lidar is the appropriate tool used to validate their model, thanks to data generated by the lidar. In terms of optimization of the wind farm operation, the nacelle-based lidar is also widely used, for turbine control, yaw misalignment or nacelle anemometer calibration.

C.2 Wind hazards monitoring for aviation weather applications

C.2.1 General

According to the state of the art and the growth of the worldwide air traffic, several projects are going on worldwide in order to renew and optimize the regulations of air traffic management (ATM), such as the Single European Sky ATM Research project in Europe^[28] and the NextGen project in the United States of America. In the field of aviation weather, two major applications have been highlighted: the measurements of wind shears and wake vortices. For these two applications, coherent Doppler lidars are now considered as well adapted and powerful sensors to improve the wind observations in order to increase safety and optimize the air traffic.

C.2.2 Wind shear

Wind shears are defined as significant changes of head- or tail-winds along the takeoff path and the approach that can affect aircrafts^[29]. These rapid changes in air speed cannot be balanced by acceleration or deceleration due to inertial effects. Thus, lift and drag, and therefore the resultant flight path, change. The effects of wind shear as mentioned above are particularly dangerous if they happen near the ground, i.e. during takeoff or landing, where they can lead to severe accidents. This is why since the conference of Chicago, the International Civil Aviation Organization (ICAO) standards have taken care of the wind shear threats to civil air traffic by mentioning wind shears in Annex 3 to the Convention on International Civil Aviation – *Meteorological Service for International Air Navigation*^[29] and by providing the ICAO *Manual on Low-level Wind Shear* (Doc 9817)^[30]. The ICAO Annex 3 distinguishes two aspects of wind shears: the wind shear alerts and wind shear warnings.

- (a) Wind shear alerts consist in providing automatic alerts of wind shear intensity observed by ground-based remote sensors. The alerts are created once wind shears are above 15 kn (7.5 m/s) in terms of headwind/tailwind changes. As detailed in reference [30], the danger of wind shears is mainly due to the strong horizontal winds that induce strong headwind and tailwind changes for the aircrafts;
- (b) Wind shear warnings must give concise information on the observed or expected existence of wind shears which could adversely affect aircraft. They are focusing below 500 m and along the takeoff path and approach. They are prepared by the meteorological office in charge of the met observations at a given airport. The wind shear warnings will be prepared "manually", thanks to all the observations (ground-based, aircrafts) and weather forecasts available.

According to the best practices, described in reference [30], coherent Doppler lidars are a good candidate technology for providing wind shear alerts and/or warnings since:

- (a) The areas of interest are the takeoff path and the approach that can be probed by a scanning coherent Doppler lidar with plan position indicator (typically with a 3° of elevation) or glide-path^[31] scans or lines of sights along the glide path;
- (b) The probing area for alerting wind shears is two extensions of 3 nautical miles of the runways, that is to say a measurement range of 7 km at least. Measurement range should be 7 km at least in appropriate atmospheric conditions (described in section 5);
- (c) The wind shear alerts are provided on the three boxes (of 1 nautical mile) that compose the extensions of each side of the runways, commonly called the ARENA (Area Noted for Attention). To compute differences of headwind or tailwind, two points are needed at a minimum. This corresponds to a theoretical required resolution better than 1.852 km. But, in order to get accurate wind shear alerts and to be able to monitor all the types of wind shears and especially the smallest ones which are the microbursts (size > 1.5 km), a range resolution of 200 m is commonly used with lidars and radars;

VOLUME III. OBSERVING SYSTEMS

- (d) ICAO documents mention the typical alert frequency suitable for the wind shears detection. In worldwide best practices, this frequency varies from 1 to 3 min;
- (e) Above all, it is important to notice that the configurations (such as accumulation time, scanning speed, alert frequency, probing area shape, probing range) of an equipment like a lidar dedicated to wind shear alerts or warnings should be adapted to the local requirements (typical local wind shear phenomena and the needs of users, such as the air traffic controllers).

Moreover, Doppler lidar systems compliant with requirements in Attachment D should be considered as a valuable supplement to Doppler weather radar observations, since they have complementary performance with respect to precipitation. Doppler lidars perform best in clear air conditions when Doppler radar receives only weak signals, and vice versa, when precipitation limits Doppler lidar observations, Doppler radar performs optimally. An example describing the setup at Hong Kong International Airport including a Doppler lidar can be found in reference [31].

C.2.3 Requirements for wake vortices detection behind aircrafts

There is strong interest of the air traffic control stakeholders for studying wake vortices because their strength (commonly characterized by their circulation) determines the minimum separation distance between aircrafts in order to ensure safety. Wake vortices consist of two strong horizontal rotational flows that trail from each wingtip. They are generated by the lift of the aircraft which induces air flow from below the wings around the wingtips into the region above the wings. The wake vortices are very stable compared to turbulence and they can last up to 3 min with stable atmospheric conditions. Their circulation is determined by the aircraft weight and air speed and by the wingspan. Their size is about 20 m but they can be very dangerous especially in the takeoff and landing phases of flight.

That is why, since the 1960s, regulations have been created by ICAO to fix the separation distances between three categories. With the increase of worldwide air traffic and the development of super heavy aircrafts, several projects aim at renewing the air traffic control regulations and especially the separation distances. Thus, plenty of wake vortices studies have been launched since the 1990s in using computational fluid dynamic models and coherent Doppler lidar technology in order to optimize the separation distances while ensuring safety^[32;33]. Scanning coherent Doppler lidars are particularly adapted to measure wake vortices since they allow to measure at high resolution below 10 m and at high frequency up to 5 s wake vortices generated by the aircraft below 500 m, for monitoring out-of-ground effects and in-ground effect wake vortex behaviour. Usually, wake vortices measurements are performed close to the runways with range height indicator scans with narrow angles of typically 10° to 40° to map vertically the motion of the wake vortices.

ELEMENT 14: Floating object (Automatic) ELEMENT 15: Picture inline Element Image: 8_II_5-C1_en.eps **END ELEMENT**

Measurement principle for determining aircraft wake vortices with Doppler wind lidar

END ELEMENT

Lidar measurements can besides be post-processed to calculate wake vortices characteristics like the probability of detection, the localization of their cores and their circulation (strength)^[34;35].

C.2.4 Siting constraints

Since the Doppler lidar delivers only the radial wind speed, siting of the instrument is a crucial point, because runway-oriented wind has to have a significant projection onto the line of sight of the lidar. In general, the magnitude, and therefore the quality, of the runway-oriented wind component projected onto the line of sight deteriorates as $\cos^2 \theta$, θ being the angle between the line of sight and the runway^[6].

Another point is that, ideally, the 3° glide slope is to be scanned. This can be ideally done with one plan position indicator scan, if the lidar is located at the runway threshold. If more than one runway threshold is to be monitored with one instrument, following exactly the 3° glide is not possible, and

CHAPTER 5. SPECIAL PROFILING TECHNIQUES FOR THE BOUNDARY LAYER AND THE TROPOSPHERE

the above-mentioned timing constraints usually do not allow scanning of more than one elevation. However, a 3° scan centred at the actual location of the lidar still outperforms an anemometerbased low-level wind shear alert system in terms of glide slope wind shear detection.

SECTION: Chapter_book Chapter title in running head: CHAPTER 5. SPECIAL PROFILING TECHNIQUES... Chapter_ID: 8_II_5_annex_en Part title in running head: PART II. OBSERVING SYSTEMS

ATTACHMENT D. TYPICAL APPLICATION RANGES AND CORRESPONDING REQUIREMENTS

(informative)

Accordingly to the needs for the main applications (see table below), three accuracy classes for the wind velocity are being defined. These classes are related to a defined spatial and temporal resolution. The wind velocity accuracy must be ensured in all ranges of interest.

- (a) Class A: $x \le 0.1$ m/s (e.g. for wind energy purposes);
- (b) Class B: $0.1 < x \le 0.5$ m/s (e.g. for meteorological applications)^[13];
- (c) Class C: $0.5 < x \le 1.0$ m/s (e.g. for nowcasting)^[13].

VOLUME III. OBSERVING SYSTEMS

SECTION: Landscape page with header_book Chapter title in running head: CHAPTER 5. SPECIAL PROFILING TECHNIQUES... Chapter_ID: 8_II_5_annex_en Part title in running head: PART II. OBSERVING SYSTEMS

Typical application ranges and corresponding requirements

TABLE: Table horizontal lines

Application	Parameter to be provided	Reference	Typical probing range (m)	Range resolution (m)	Time resolution (min)	Velocity measurement accuracy (m/s)	Wind direction accuracy (°)	Minimum data availability (%)
Radial velocity mapping	Line-of-sight radial velocity	Formula 5.A.5	200-10 000	25-100	1-10	0.5	Not applicable	50-99ª
Wind energy, e.g. site assessment, power curve, wind profile	d ^{Profile} of the horizontal wind vector along the vertical axis	e.g. [36]	40-200	25	10	0.5	2	85
High-resolution numerical weather prediction	Profile of the horizontal wind vector along the vertical axis	[13]	> 50	25	10	0.5	2	80
Air pollution, e.g. dispersion modelling, risk management	Profile of the horizontal wind vector along the vertical axis	2	40-200	25	10	0.5	-	90
Aviation: wind shear	Radial wind along takeoff path, approach and runways	[29;36]	7 000-8 000 (5 500 + half the runway)	200	1	0.5	5	80

CHAPTER 5. SPECIAL PROFILING TECHNIQUES FOR THE BOUNDARY LAYER AND THE TROPOSPHERE

Aviation: vortex monitoring (ground-based systems)	Radial wind speed in perpendicular planes to the runway	_	Distance to runway + 300–500 on each side	25 (5 with overlap)	0.1	1	-	< 50
Met applications, e.g. nowcasting	Profile of the horizontal wind vector along the vertical axis	[13]	0-4 000	100	15	I	5	80
a Depending on application					0			
				5				
			$\overline{\mathbf{O}}$					
	. (
	$\langle \circ \rangle$							

SECTION: Chapter_book Chapter title in running head: CHAPTER 5. SPECIAL PROFILING TECHNIQUES... Chapter_ID: 8_II_5_annex_en Part title in running head: PART II. OBSERVING SYSTEMS BIBLIOGRAPHY

[1] Henderson, S.W., P. Gatt, D. Rees and R.M.N. Huffaker, 2005: Wind lidar. In: *Laser Remote Sensing* (T. Fujii and T. Fukuchi, eds.). 469–722, CRC Press, ISBN-10: 8247-4256-7.

- [2] Measures, R.M., 1992: *Laser Remote Sensing: Fundamentals and Applications*. Krieger Publishing, 524 pp., ISBN-10: 8946-4619-2.
- [3] Frehlich, R. and M. Kavaya, 1991: Coherent laser radar performance for general atmospheric refractive turbulence. *Appl. Opt.*, 30:5325–5352.
- [4] Belmonte, A., 2003: Analyzing the efficiency of a practical heterodyne lidar in the turbulent atmosphere: telescope parameters. *Opt. Express.*, 11:2041–2046.
- [5] Frehlich, R., S. Hannon and S. Henderson, 1997: Coherent Doppler lidar measurements of winds in the weak signal regime. *Appl. Opt.*, 36:3491–3499.
- [6] Banakh, V.A. and I.N. Smalikho, 1997: Estimation of the turbulence eddy dissipation rate from the pulsed Doppler lidar data. *Atmos. Oceanic Opt.*, 10(12).
- [7] Frehlich, R., 1996: Simulation of coherent Doppler lidar performance in the weak signal regime. *J. Atmos. Ocean. Technol.*, 13:646–658.
- [8] Dabas, A., P. Drobinski and P. Flamant, 2000: Velocity biases of adaptive filters in heterodyne doppler lidar measurements. *J. Atmos. Ocean. Technol.*, 17:1189–1202.
- [9] Dabas, A., 1999: Semi empirical model for the reliability of a matched filter frequency estimator for Doppler lidar. *J. Atmos. Ocean. Technol.*, 16:19–28.
- [10] Goodman, J.W., 1975: Statistical properties of laser speckle patterns. In: *Laser Speckle* (J.C. Dainty, ed.). Springer.
- [11] American National Standards Institute (ANSI) Z136.1-2014: American National Standard for Safe Use of Lasers. ISBN: 978-1-940168-00-5.
- [12] IEC 60825-1:2014: Safety of Laser Products Part 1: Equipment Classification and Requirement.
- [13] World Meteorological Organization: http://www.wmo-sat.info/oscar/requirements.
- [14] Boquet, M., P. Royer, J.P. Cariou, M. Machta and M. Valla, 2016: Simulation of doppler lidar measurement range and data availability. *J. Atmos. Ocean. Technol.*, paper accepted, DOI: 10.1175/JTECH-D-15-0057.1.
- [15] Frehlich, R., 2001: Estimation of velocity error for doppler lidar measurements. *J. Atmos. Ocean. Technol.*, 18:1628–1639.
- [16] Ernsdorf, T., B. Stiller, B.R. Beckmann, A. Weipert, S. Kauczok and R. Hannesen, 2014: Intercomparison of X-band radar and lidar low-level wind measurement for air traffic control (ATC). Eighth Europ. Conf. on Radar in Meteorol. and Hydrol., Garmisch-Partenkirchen, Germany.
- [17] Hannesen, R., S. Kauczok and A. Weipert, 2014: Quality of clear-air radar radial velocity data: do insects matter? Eighth Europ. Conf. on Radar in Meteorol. and Hydrol., Garmisch-Partenkirchen, Germany.
- [18] Weipert, A., S. Kauczok, R. Hannesen, T. Ernsdorf and B. Stiller, 2014: Wind shear detection using radar and lidar at Frankfurt and Munich airports. Eighth Europ. Conf. on Radar in Meteorol. and Hydrol., Garmisch-Partenkirchen, Germany.
- [19] Jörgensen, H., T. Mikkelsen, J. Streicher, H. Herrmann, C. Werner and E. Lyck, 1997: Lidar calibration experiment. *Appl. Phys. B.*, 64:355–361.
- [20] Bronstein, I.N., K.A. Semendjajew, G. Musiol and H. Mühlig, 1993: *Taschenbuch der Mathematik*. Harri Deutsch.

- [21] Fukao, S. and K. Hamazu, 2013: *Radar for Meteorological and Atmospheric Observations*. Springer.
- [22] Banakh, V.A. and I.N. Smalikho, 2013: *Coherent Doppler Wind Lidars in a Turbulent Atmosphere.* Artech House.
- [23] Srinivaso, R.I., V.K. Anandan and R.R. Narasimha, 2008: Evaluation of DBS wind measurement technique in different beam configurations for a VHF wind profiler. *J. Atmos. Ocean. Technol.*, 25(12):2304–2312.
- [24] Lhermite, R.M., 1962: Note on wind variability with Doppler radar. J. Atmos. Sci., 19(4):343–346.
- [25] Browning, K.A. and R. Wexler, 1968: The determination of kinematic properties of a wind field using Doppler radar. *J. Appl. Meteorol.*, 7(1):105–113.
- [26] Waldteufel, P. and H. Corbin, 1979: On the analysis of single Doppler radar data. *J. Appl. Meteor.*, 18:532–542.
- [27] IEC 61400-12-1:2005: Wind Turbines Part 12-1: Power Performance Measurements of Electricity Producing Wind Turbines.
- [28] European ATM Master Plan, 2009: https://www.atmmasterplan.eu/.
- [29] International Civil Aviation Organization, 2007: *Meteorological Service for International Air Navigation*, Annex 3 to the Convention on International Civil Aviation.
- [30] International Civil Aviation Organization, 2005: *Manual on Low-level Wind Shear*, Doc 9817 AN/449.
- [31] Shun, C.M. and P.W. Chan, 2008: Applications of an infrared doppler lidar in detection of wind shear. *J. Atmos. Ocean. Technol.*, 25(5):637–655.
- [32] Wakenet-Eu: http://www.wakenet.eu/.
- [33] Lang, S. and W. Bryant, 2006: *Vortex Research in the USA (WakeNet-USA)*. Air Traffic Organization, Federal Aviation Administration.
- [34] Holzäpfel, F., T. Gerz, F. Köpp, E. Stumpf, M. Harris, R.I. Young and A. Dolfi-Bouteyre, 2003: Strategies for circulation evaluation of aircraft wake vortices measured by lidar. *J. Atmos. Ocean. Technol.*, 20(8):1183–1195.
- [35] Dolfi-Bouteyre, A., B. Augere, M. Valla, D. Goular, D. Fleury and G. Canat, 2009: 1,55 μ m pulsed fiber lidar for wake vortex detection (axial or transverse). Wakenet-Eu Workshop.
- [36] Hasager, C.B., D. Stein, M. Courtney, A. Pena, T. Mikkelsen, M. Stickland and A. Oldroyd, 2013: Hub height ocean winds over the North Sea observed by the NORSEWIND lidar array: measuring techniques, quality control and data management. *Remote Sens.*, 5:4280–4303.
- [37] ISO 28902-1: Air Quality Environmental Meteorology Part 1: Ground-based Remote Sensing of Visual Range by Lidar.
- [38] ISO 28902-3:⁴ Air Quality Environmental Meteorology Part 3: Ground-based Remote Sensing of Wind by Continuous-wave Doppler Lidar.

SECTION: Chapter_book Chapter title in running head: CHAPTER 5. SPECIAL PROFILING TECHNIQUES... Chapter_ID: 8_II_5_en Part title in running head: PART II. OBSERVING SYSTEMS

⁴ Under preparation

REFERENCES AND FURTHER READING

- Adachi, A., T. Kobayashi, K.S. Gage, D.A. Carter, L.M. Hartten, W.L. Clark and M. Fukuda, 2005: Evaluation of three-beam and four-beam profiler wind measurement techniques using a five-beam wind profiler and collocated meteorological tower. *Journal of Atmospheric and Oceanic Technology*, 22:1167–1180.
- Angevine, W.M., W.L. Ecklund, D.A. Carter, K.S. Gage and K.P. Moran, 1994: Improved radio acoustic sounding techniques. *Journal of Atmospheric and Oceanic Technology*, 11(1):42–49.
- Bianco, L., D. Gottas and J.M. Wilczak, 2013: Implementation of a Gabor transform data quality-control algorithm for UHF wind profiling radars. *Journal of Atmospheric and Oceanic Technology*, 30(12): 2697-2703.
- Bevis, M., S. Businger, S. Chiswell, T.A. Herring, R.A. Anthes, C. Rocken and R.H. Ware, 1994: GPS meteorology: Mapping zenith wet delays onto precipitable water. *Journal of Applied Meteorology*, 33:379–386.
- Brown, E.H. and F.F. Hall, 1978: Advances in atmospheric acoustics. *Reviews of Geophysics and Space Physics*, 16:47–109.
- Cadeddu, M.P., G.E. Peckham and C. Gaffard, 2002: The vertical resolution of ground-based microwave radiometers analyzed through a multiresolution wavelet technique. *IEEE Transactions on Geoscience and Remote Sensing*, 40(3):531–540.
- Candlish, L.M., R.L. Raddatz, M.G. Asplin and D.G. Barber, 2012: Atmospheric temperature and absolute humidity profiles over the Beaufort Sea and Amundsen Gulf from a microwave radiometer. *Journal* of Atmospheric and Oceanic Technology, 29:1182–1201.
- Chan, P.W., 2009: Performance and application of a multi-wavelength, ground-based microwave radiometer in intense convective weather. *Meteorologische Zeitschrift*, 18:253-265.
- Chan, P.W. and Y.F. Lee, 2013: Application of brightness temperature data from a ground-based microwave radiometer to issue low-level windshear alert over Hong Kong International Airport. *Mausam* <u>64:457-466.</u>
- Chan, W.S. and J.C.W. Lee, 2015: Vertical profile retrievals with warm-rain microphysics using the groundbased microwave radiometer operated by the Hong Kong Observatory. *Atmos. Res.*, 161-162:125-133.
- Chakraborty, R., S. Das and A. Maitra, 2016: Prediction of convective events using multi-frequency radiometric observations at Kolkata. *Atmos. Res.*, 169:24-31.
- <u>Chakraborty, R., S. Das and A. Maitra, 2016: Prediction of convective events using multi-frequency</u> radiometric observations at Kolkata. *Atmos. Res.*, 169:24-31.
- Davis, J.L., T.A. Herring, I.I. Shapiro, A.E.E. Rogers and G. Elgered, 1985: Geodesy by radio interferometry: Effects of atmospheric modeling errors on estimates of baseline length. *Radio Science*, 20(6):1593–1607.
- Derr, V.E., 1972: *Remote Sensing of the Troposphere*. United States National Oceanic and Atmospheric Administration, WPL, Boulder, Colorado.
- Dolman, B. K. and I.M. Reid, 2014: Bias correction and overall performance of a VHF spaced antenna boundary layer profiler for operational weather forecasting. *Journal of Atmospheric and Solar-Terrestrial Physics*, 118:16-24.
- Doviak, R. J. and D.D. Zrnic, 2014: Doppler Radar & Weather Observations. Academic Press.

Elgered, G., H.-P. Plag, S. Barlag and J. Nash, 2004: COST716 Final Report, European Union.

- <u>Fernández-González, S., F. Valero, J.L. Sanchez, E. Gascon, L. Lopez, E. Garcia-Ortega, and A. Merino, 2014:</u> <u>Observation of a freezing drizzle episode: A case study. *Atmos. Res.*, 149:244-254.</u>
- Fukao, S., K. Hamazu and R.J. Doviak, 2014: Radar for meteorological and atmospheric observations. Springer Japan.

- Gaffard, C. and T. Hewison, 2003: Radiometrics MP3000 microwave radiometer trial report. *Technical Report* -*TR26*, Met Office, Workingham, Berkshire, UK.
- Gaynor, J.E., C.B. Baker and J.C. Kaimal, 1990: The international sodar intercomparison experiment. *Proceedings of the Fifth International Symposium on Acoustic Remote Sensing*. McGraw-Hill, New York, pp. 67–74.
- Gossard, E.E. and R.G. Strauch, 1983: *Radar Observations of Clear Air and Clouds*. Elsevier, Scientific Publishing Co., Amsterdam.
- Güldner, J. and D. Spänkuch, 2001: Remote sensing of the thermodynamic state of the atmospheric boundary layer by ground-based microwave radiometry. *Journal of Atmospheric and Oceanic Technology*, 18:925–933.
- Hinkley, E.D., 1976: *Laser Monitoring of the Atmosphere: Topics in Applied Physics*. Volume 14, Springer Verlag, New York.

Hogg, D.C., M.T. Decker, F.O. Guiraud, K.B. Earnshaw, D.A. Merritt, K.P. Moran, W.B. Sweezy, R.G. Strauch, E.R. Westwater and C.G. Little, 1983: An automatic profiler of the temperature, wind and humidity in the troposphere. *Journal of Climate and Applied Meteorology*, 22:807–831.

- Hocking, W.K., 2011: A review of mesosphere-stratosphere-troposphere (MST) radar developments and studies, circa 1997–2008. Journal of Atmospheric and Solar-Terrestrial Physics, 73(9):848-882.
- Hocking, W.K., T. Sato, R. D. Palmer, J. Röttger, P.B. Chilson (2016): Atmospheric Radar: Application and Science of MST Radars in the Earth's Mesosphere, Stratosphere, Troposphere, and Weakly Ionized Regions. Cambridge University Press.
- Illingworth, A. J., D. Cimini, C. Gaffard, M. Haeffelin, V. Lehmann, U. Löhnert and D. Ruffieux, 2015: Exploiting existing ground-based remote sensing networks to improve high-resolution weather forecasts. Bulletin of the American Meteorological Society, 96(12):2107-2125.
- Kadygrov, E.N., E.A. Miller and A.V. Troitsky, 2013: Study of atmospheric boundary layer thermodynamics during total solar eclipses. *IEEE Transactions on Geoscience and Remote Sensing*, 51(9):4672–4677.
- Kadygrov, E.N. and D.R. Pick, 1998: The potential for temperature retrieval from an angular-scanning singlechannel microwave radiometer and some comparisons with in situ observations. *Meteorological Applications*, 5:393–404.
- Kadygrov, E.N., G.N. Shur and A.S. Viazankin, 2003: Investigation of atmospheric boundary layer temperature, turbulence, and wind parameters on the basis of passive microwave remote sensing. *Radio Science*, 38(3):13.1–13.12.
- Lataitis, R.J., 1992a: Signal power for radio acoustic sounding of temperature: The effects of horizontal winds, turbulence and vertical temperature gradients. *Radio Science*, 27:369–385.
- ----, 1992b: Theory and Application of a Radio-acoustic Sounding System. NOAA Technical Memorandum ERL WPL-230.
- Liljegren, J.C., S.A. Boukabara, K. Cady-Pereira and S.A. Clough, 2005: The Effect of the half-width of the 22-GHz water vapor line on retrievals of temperature and water vapor profiles with a 12-channel radiometer. *IEEE Transactions on Geoscience and Remote Sensing*, 43(5):1102–1108.
- Madhulatha, A., M. Rajeevan, M.V. Ratnam, J. Bhate and C.V. Naidu, 2013: Nowcasting severe convective activity over southeast India using ground-based microwave radiometer observations. *Journal of Geophysical Research: Atmospheres*, 118(1):1–13.
- Martner, B.E., D.B. Wuertz, B.B. Stankov, R.G. Strauch, E.R. Westwater, K.S. Gage, W.L. Ecklund, C.L. Martin and W.F. Dabberdt, 1993: An evaluation of wind profiler, RASS and microwave radiometer performance. *Bulletin of the American Meteorological Society*, 74(4):599–613.
- May, P.T., R.G. Strauch, K.P. Moran and W.L. Eckund, 1990: Temperature sounding by RASS, with wind profiler radars: A preliminary study. *IEEE Transactions on Geoscience and Remote Sensing*, 28(1):19–28.
- Muschinski, A., V. Lehmann, L. Justen and G. Teschke, 2005; Advanced radar wind profiling. *Meteorologische* Zeitschrift, 14(5):609-625.

- Navas-Guzman, F., O. Stahli and N. Kampfer, 2013: Study of cloud effect on the tropospheric temperature retrievals. In: URSI Commission F Microwave Signatures 2013: Specialist Symposium on Microwave Remote Sensing of the Earth, Oceans, and Atmosphere, October 2013, Finland, p.136.
- Neff, W.D. and R.L. Coulter, 1986: Acoustic remote sounding. In: *Probing the Atmospheric Boundary Layer* (Lenschow, D.H., ed.). American Meteorological Society, 201–236.
- Panofsky, H.A., 1973: Tower micrometeorology. In: *Workshop on Micrometeorology* (Haugen, D.A., ed.), Chapter 4, American Meteorological Society.
- Saastamoinen, J., 1972: Atmospheric correction for the troposphere and stratosphere in radio ranging of satellites. *Geophysical Monograph Series: The Use of Artificial Satellites for Geodesy*, 15:247–251.
- Singal, S.P., 1990: Current status of air quality related boundary layer meteorological studies using sodar. *Proceedings of the Fifth International Symposium on Acoustic Remote Sensing*, McGraw-Hill, New York, 453–476.
- Smith, E.K. and S. Weintraub, 1953: The constants in the equation for atmospheric refractive index at radio frequencies. *Proceedings of the IRE*, 41(8):1035–1037.
- Solheim, F., J.R. Godwin, E.R. Westwater, Y. Han, S.J. Keihm, K. Marsh, R. Ware, 1998: Radiometric profiling of temperature, water vapor, and cloud liquid water using various inversion methods. *Radio Science*, 33:393–404.
- Syed, I. and E.V. Browell, 1994: Recent Lidar technology developments and their influence on measurements of tropospheric water vapor. *Journal of Atmospheric and Oceanic Technology*, 11(1):76–84.
- <u>Teschke, G. and V. Lehmann, 2017: Mean wind vector estimation using the velocity-azimuth display (VAD)</u> <u>method: an explicit algebraic solution. *Atmospheric Measurement Techniques*, 10:3265–3271.</u>
- Thayer, G.D., 1974: An improved equation for the radio refractive index of air. *Radio Science*, 9(10):803–807.
- Thomas, L., 1991: Lidar probing of the atmosphere. *Indian Journal of Radio and Space Physics*, 20:368–380.
- Thompson, A.R., J.M. Moran and G.W. Swenson, 1986: *Interferometry and Synthesis in Radio Astronomy*. John Wiley and Sons, New York.
- Thompson, N., 1980: Tethered balloons. In: *Air-sea Interaction: Instruments and Methods* (F. Dobson, L. Hasse and R. Davis, eds.) Chapter 31, Plenum Press, New York.
- <u>Wakasugi, K., and S. Fukao, 1985: Sidelobe properties of a complementary code used in MST radar</u> observations. *IEEE Transactions on Geoscience and Remote Sensing*, 1:57-59.
- Ware, R., R. Carpenter, J. Güldner, J. Liljegren, T. Nehrkorn, F. Solheim and F. Vandenberghe, 2003: A multi-channel radiometric profiler of temperature, humidity and cloud liquid. *Radio Science*, 38:8079–8092.
- Ware, R., D. Cimini, E. Campos, G. Giuliani, S. Albers, M. Nelson, S.E. Koch, P. Joe and S. Cober, 2013: Thermodynamic and liquid profiling during the 2010 Winter Olympics. *Atmospheric Research*, 132– 133:278–290.
- Weber, B.L. and D.B. Wuertz, 1990: Comparison of rawinsonde and wind profiler radar measurements. Journal of Atmospheric and Oceanic Technology, 7(1):157–174.
- Weber, B.L., D.B. Wuertz, R.G. Strauch, D.A. Merritt, K.P. Moran, D.C. Law, D. van de Kamp, R.B. Chadwick, M.H. Ackley, M.F. Barth, N.L. Abshire, P.A. Miller and T.W. Schlatter, 1990: Preliminary evaluation of the first NOAA demonstration network wind profiler. *Journal of Atmospheric and Oceanic Technology*, 7(6):909–918.
- Westwater, E., S. Crewell, C. Mätzler and D. Cimini, 2005: Principles of Surface-based Microwave and Millimeter Wave Radiometric Remote Sensing of the Troposphere. *Quaderni Della Società Italiana di Elettromagnetismo*, 1(3).
- Westwater, E.R., Y. Han, V.G. Irisov, V. Leuskiy, E.N. Kadygrov and S.A. Viazankin, 1999: Remote sensing of boundary layer temperature profiles by a scanning 5-mm microwave radiometer and RASS: Comparison experiments. *Journal of Atmospheric and Oceanic Technology*, 16:805–818.

- Westwater, E.R., J.B. Snider and M.J. Falls, 1990: Ground-based radiometric observations of atmospheric emission and attenuation at 20.6, 31.65, and 90.0 GHz: A comparison of measurements and theory. *IEEE Transactions on Antennas and Propagation*, 38(10):1569–1580.
- <u>Wilczak, J. M., E.E. Gossard, W.D. Neff and W.L. Eberhard, 1996: Ground-based remote sensing of the</u> <u>atmospheric boundary layer: 25 years of progress. In *Boundary-Layer Meteorology 25th* <u>Anniversary Volume, 1970–1995:321-349, Springer Netherlands.</u></u>
- <u>Woods, C.P., Stoelinga, M.T., Locatelli, J.D., Hobbs, P.V., 2005 Microphysical processes and synergistic</u> <u>interaction between frontal and orographic forcing of precipitation during the 13 December 2001</u> <u>IMPROVE-2 event over the Oregon Cascades. J. Atmos. Sci., 62(10):3493-3519.</u>
- World Meteorological Organization, 1980: Lower Tropospheric Data Compatibility: Low-level Intercomparison Experiment (Boulder, United States, 1979). Instruments and Observing Methods Report No. 3. Geneva.
- ———, 1982: Indirect Sensing: Meteorological Observations by Laser Indirect Sensing Techniques (A.O. Van Gysegem). Instruments and Observing Methods Report No. 12. Geneva.
- , 1994: Comparison of windprofiler and rawinsonde measurements (J. Neisser, V. Görsdorf and H. Steinhagen). Papers Presented at the WMO Technical Conference on Instruments and Methods of Observation (TECO-94). Instruments and Observing Methods Report No. 57 (WMO/TD-No. 588). Geneva.
- ———, 2006a: Operational Aspects of Different Ground-Based Remote Sensing Observing Techniques for Vertical Profiling of Temperature, Wind, Humidity and Cloud Structure: A Review (E.N. Kadygrov). Instruments and Observing Methods Report No. 89 (WMO/TD-No. 1309). Geneva.
- ———, 2006b: National/Regional Operational Procedures of GPS Water Vapour Networks and Agreed International Procedures (S. de Haan). Instruments and Observing Methods Report No. 92 (WMO/TD-No. 1340). Geneva.
- Xu, G., R. Ware, W. Zhang, and G. Feng, 2014: Effect of the off-zenith observation on reducing the impact of precipitation on ground-based microwave radiometer measurement accuracy in Wuhan. *Atmos. Res.* 140-141:85-94.